

# **Special Topics in Particle Physics**

## **Secondary Cosmic Rays**

**Helga Dénés 2024 S1 Yachay Tech**

[hdenes@yachaytech.edu.ec](mailto:hdenes@yachaytech.edu.ec)

**Fig. 7.4** Transformation of primary cosmic rays in the atmosphere

# Extensive air showers

**Extensive air showers** are cascades initiated by energetic primary particles, which develop in the atmosphere. An extensive air shower (EAS) has an electromagnetic, a muonic, a hadronic, and a neutrino component (see Fig. 7.4).

The air shower develops a **shower nucleus consisting of energetic hadrons**, which permanently **inject energy into** the electromagnetic and **the other shower components** via interactions and decays.

**Neutral pions**, which are produced in nuclear interactions and whose decay photons produce electrons and positrons via pair production, supply the electron, positron, and photon component.

**Photons, electrons, and positrons initiate electromagnetic cascades** through alternating processes of pair production and bremsstrahlung.

The **muon and neutrino components** are formed by the **decay of charged pions and kaons** (see also Fig. 7.4).

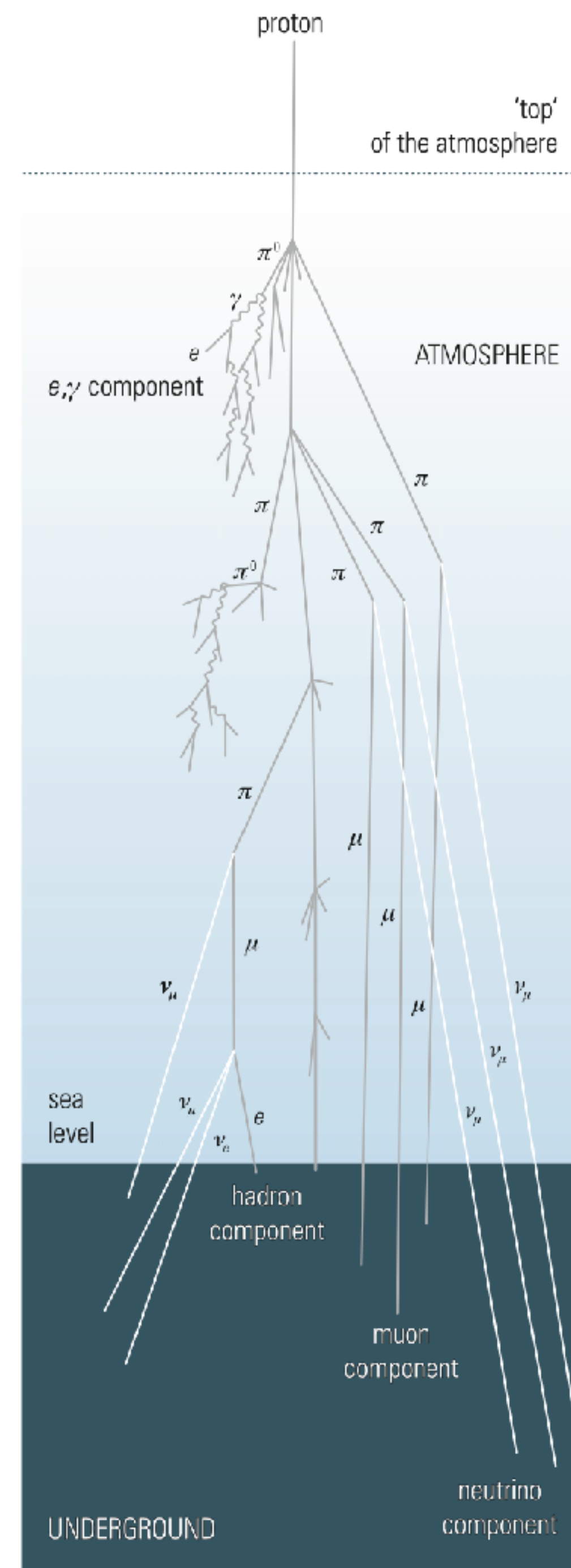


**Fig. 7.4** Transformation of primary cosmic rays in the atmosphere

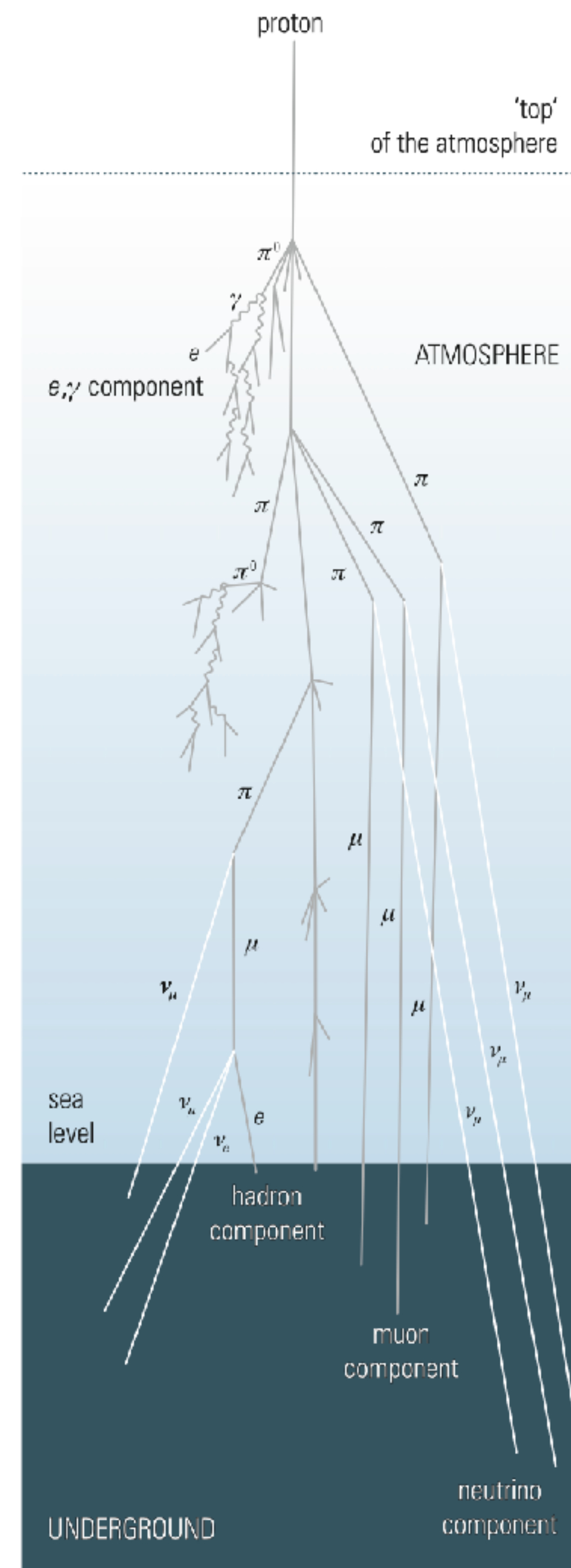
# Extensive air showers

The **inelasticity in hadron interactions is on the order of 50%**, i.e., 50% of the primary energy is transferred into the **production of secondary particles**.

Since **predominantly pions are produced** ( $N(\pi) : N(K) = 9 : 1$ ) and all charge states of pions ( $\pi^+$ ,  $\pi^-$ ,  $\pi^0$ ) are produced in equal amounts, **one third of the inelasticity is transferred into the formation of the electromagnetic component**.

Since most of the charged hadrons produced also undergo multiple interactions, the **largest fraction of the primary energy is eventually transferred into the electromagnetic cascade**. Therefore, **in terms of the number of particles, electrons and positrons constitute the main shower component**.

The **particle number increases with shower depth  $t$  until absorptive processes like ionization for charged particles and Compton scattering and photoelectric effect for photons start to dominate and cause the shower to die out**.



# Extensive air showers

The **development of electromagnetic cascades** is shown in Fig. 7.25 for various primary energies.

The **particle intensity increases initially in a parabolic fashion and decays exponentially after the maximum** of the shower has been reached.

The **longitudinal profile of the particle number** can be parameterized by

$$N(t) \sim t^\alpha e^{-\beta t}$$

where  $t = x/X_0$  is the **shower depth** in units of the radiation length and  $\alpha$  and  $\beta$  are free fit parameters.

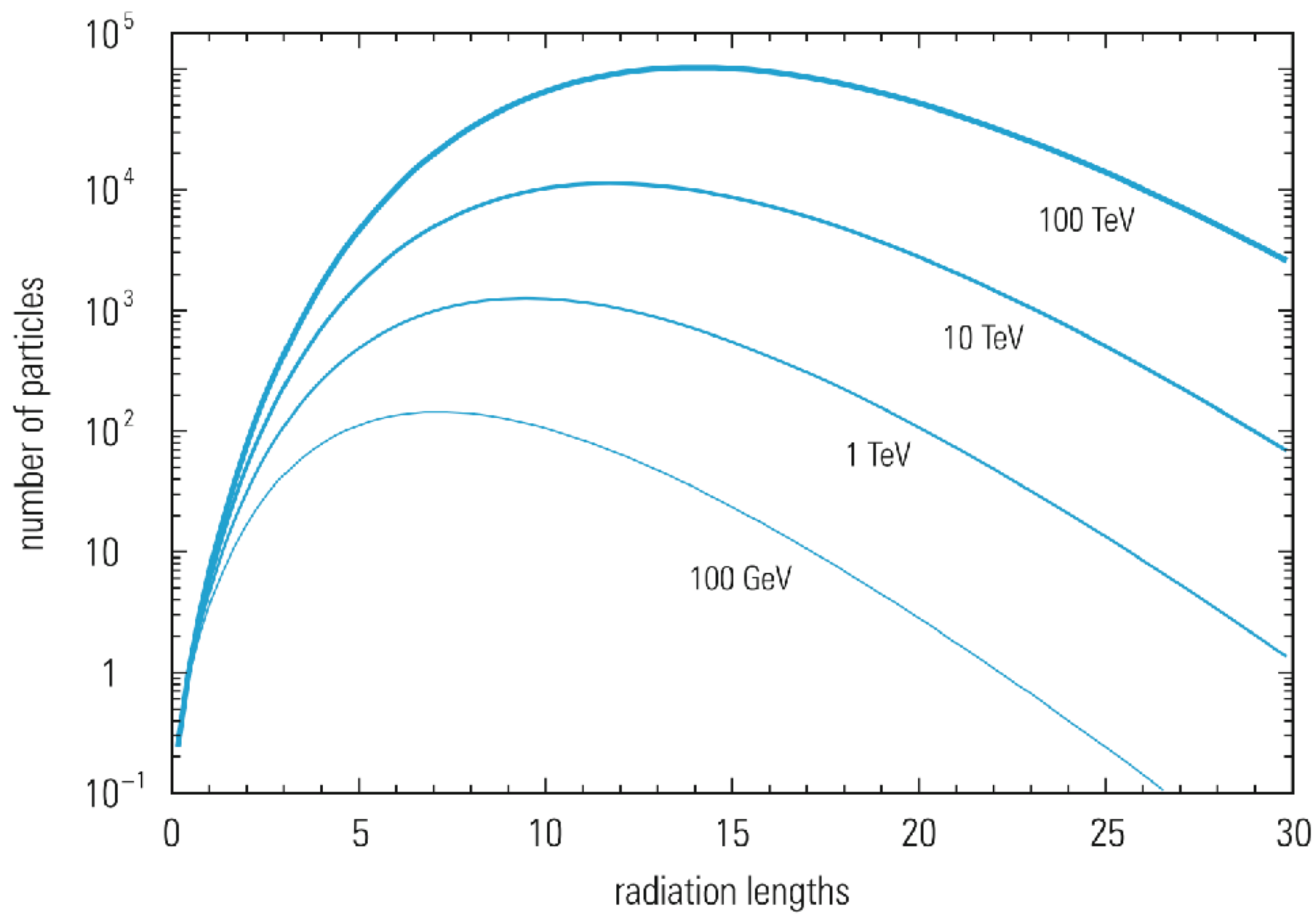


**Fig. 7.25** Longitudinal development of electromagnetic cascades. The shower depth is given in units of the radiation length. The atmosphere comprises 27 radiation lengths [124]

# Extensive air showers

The position of the shower maximum varies only logarithmically with the primary energy, while the **total number of shower particles increases linearly with the energy**. The latter can therefore be used for the **energy determination of the primary particle**.

One can imagine that the Earth's atmosphere represents a **combined hadronic and electromagnetic calorimeter**, in which the extensive air shower develops. The atmosphere constitutes approximately a target of **11 interaction lengths and 27 radiation lengths**.

The **minimum energy for a primary particle to be reasonably well measured** at sea level via the particles produced in the air shower is about  **$10^{14}$  eV = 100 TeV**.

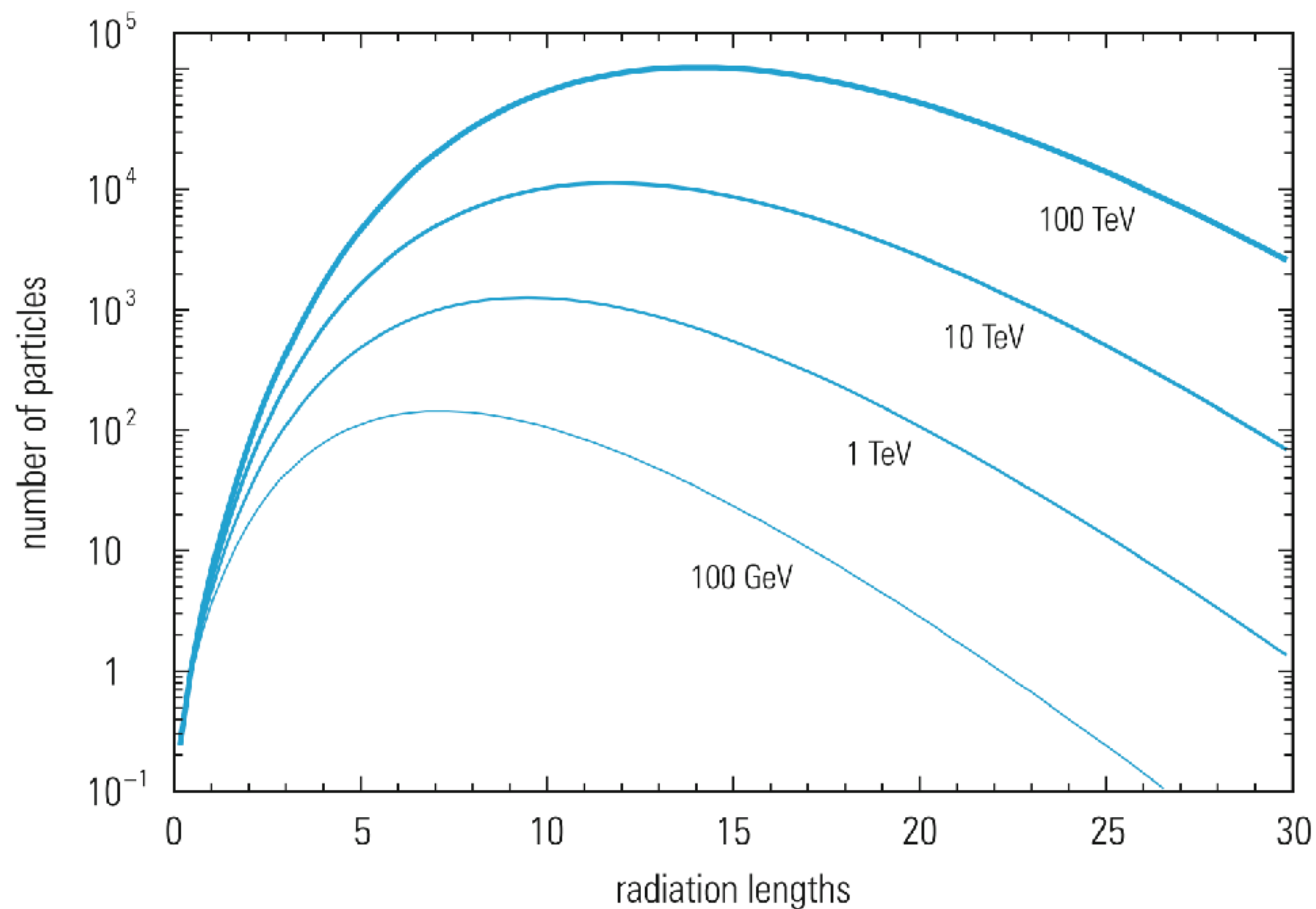


**Fig. 7.25** Longitudinal development of electromagnetic cascades. The shower depth is given in units of the radiation length. The atmosphere comprises 27 radiation lengths [124]

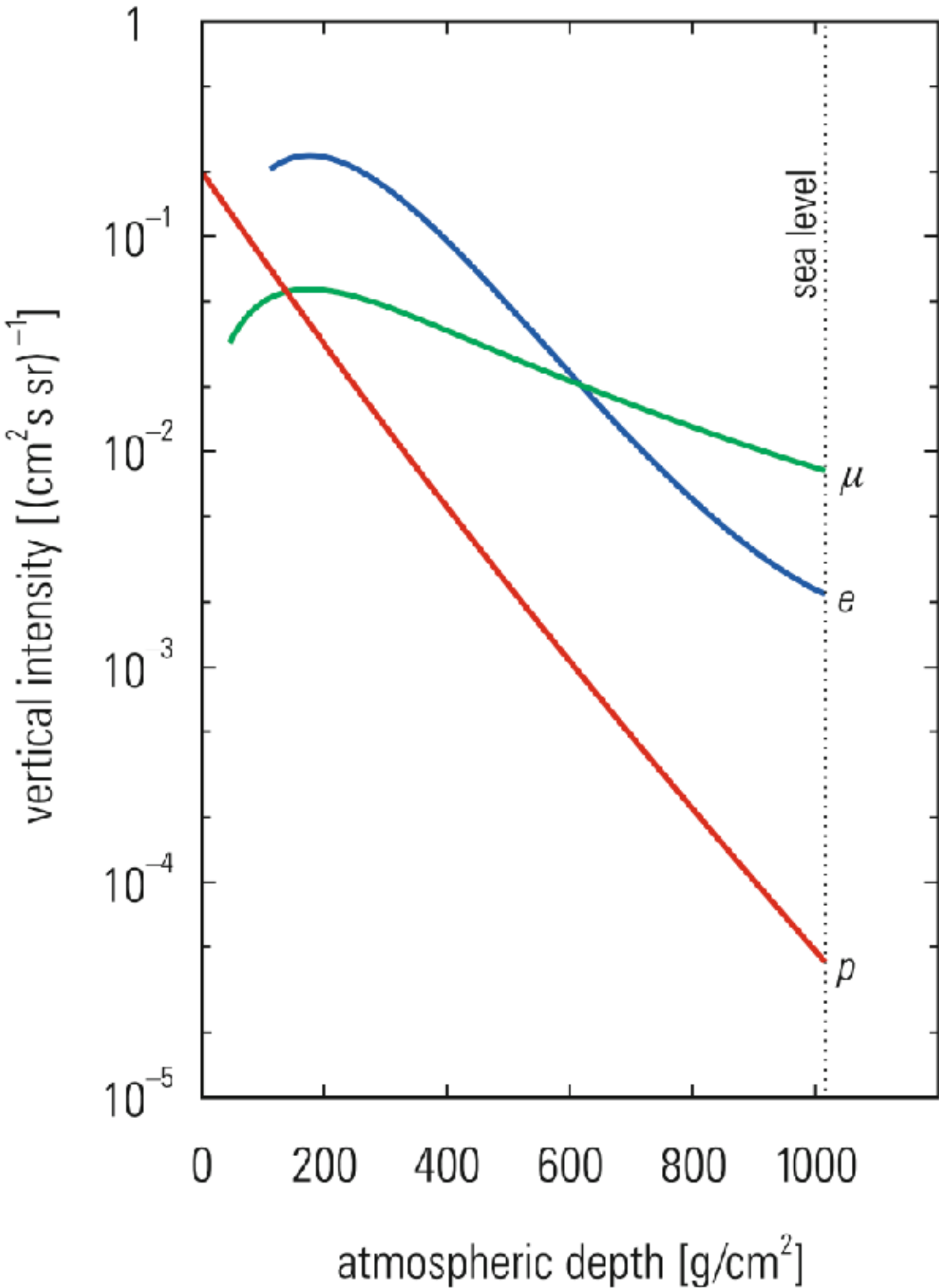
# Extensive air showers

As a rough estimate for the particle number  $N$  at sea level in its dependence on the primary energy  $E_0$ , one can use the relation

$$N = 10^{-10} E_0 [\text{eV}]$$

Only **about 10% of the charged particles in an extensive air shower are muons**. The number of muons reaches a plateau already at an atmospheric depth of  $200 \text{ g/cm}^2$  (see also Figs. 7.9 and 7.10). Its **number is hardly reduced to sea level**, since the probability for catastrophic energy-loss processes, like bremsstrahlung, is low compared to electrons because of the large muon mass. Muons also lose only a small fraction of their energy by ionization. Because of the relativistic time dilation the decay of energetic muons ( $E\mu > 3 \text{ GeV}$ ) in the atmosphere is strongly suppressed.

**Fig. 7.9** Particle composition in the atmosphere as a function of atmospheric depth [112]



# Extensive air showers

Figure 7.26 shows schematically the **longitudinal development of the various components of an extensive air shower** in the atmosphere for a primary energy of  $10^{19}$  eV. The **lateral spread** of an extensive air shower is essentially **caused by the transferred transverse momenta in hadronic interactions and by multiple scattering of low-energy shower particles**.

The muon component is somewhat flatter compared to the lateral distribution of electrons and hadrons.

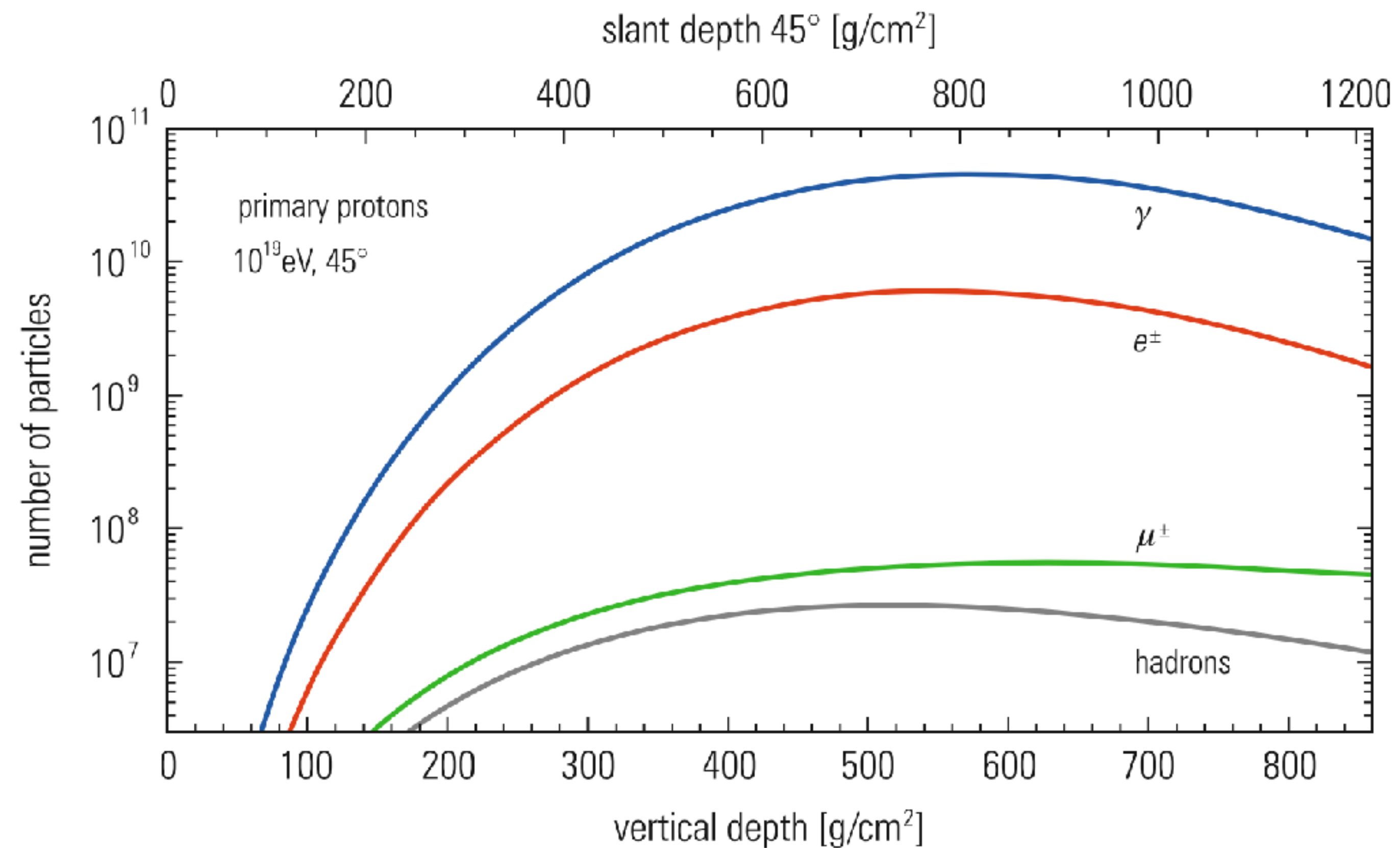


**Fig. 7.26** Longitudinal development of different particle species in an air shower of  $10\text{ EeV}$  energy for a zenith angle of  $45^\circ$  [125]

# Extensive air showers

Figure 7.27 shows the lateral particle profile for the various shower components. Neutrinos essentially follow the shape of the muon component.

Even though an extensive air shower initiated by primary particles with **energies below 100TeV does not reach sea level**, it can nevertheless be **recorded via the Cherenkov light** emitted by the shower particles. At higher energies one has the choice of various detection techniques.

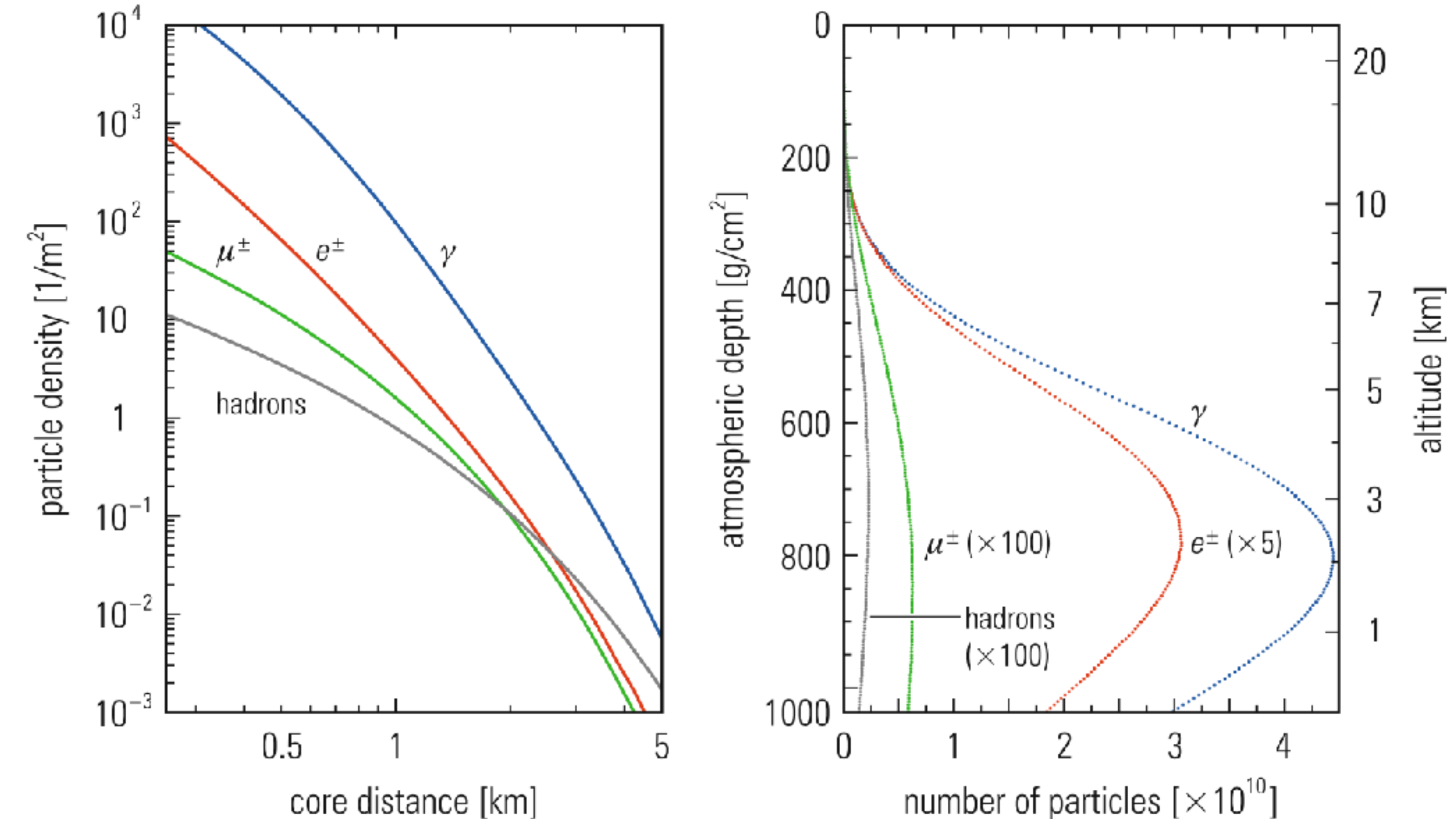
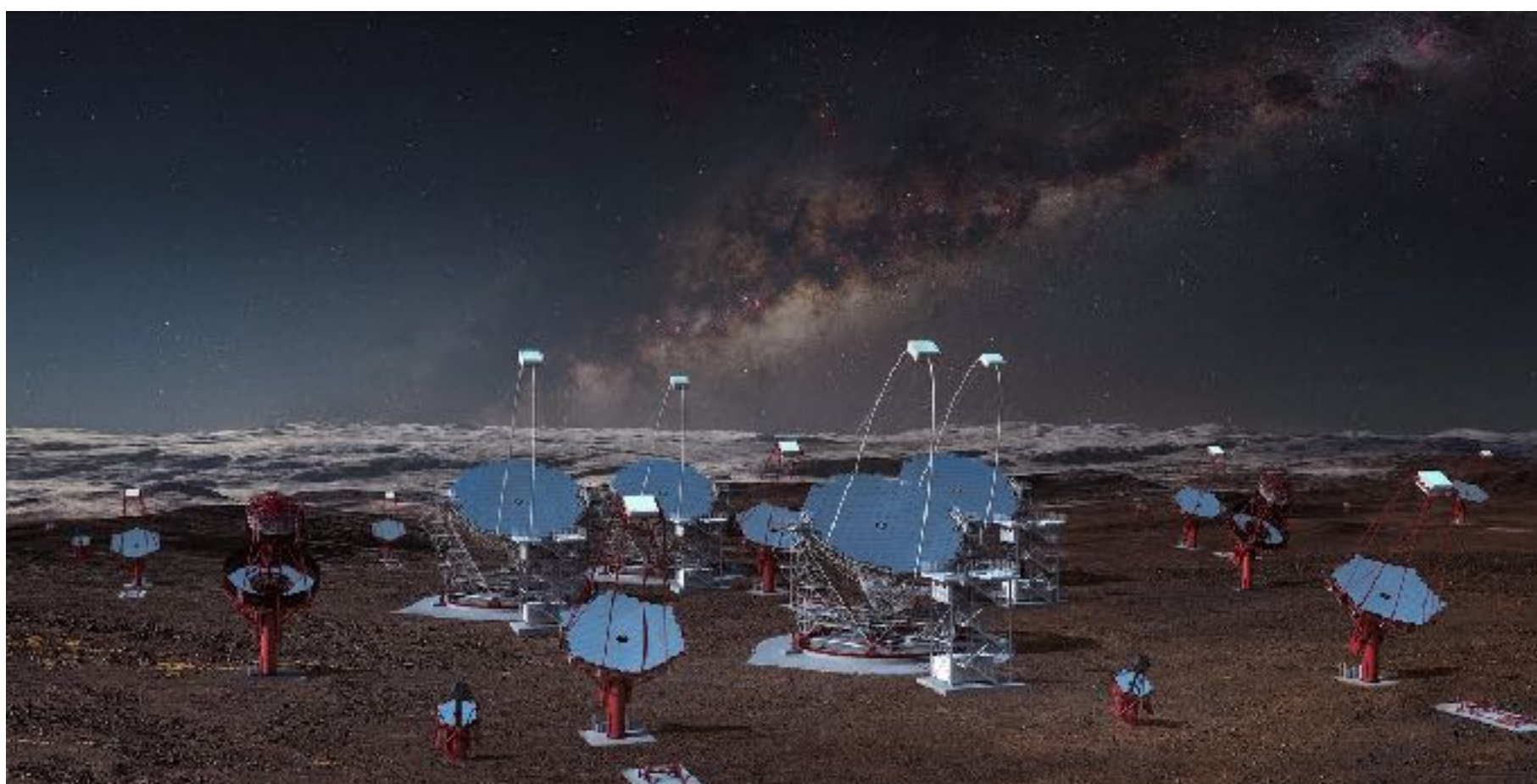


**Fig. 7.27** Lateral and longitudinal shower profiles for vertical proton-induced showers of  $10^{19}$  eV, simulated with the program CORSIKA-SIBYLL2.1. The lateral distribution of shower particles has been simulated for a shower depth of  $870 \text{ g/cm}^2$ , corresponding to the atmospheric depth of the Auger experiment for vertical incidence. The energy thresholds for secondary particles are 0.25 MeV for photons, electrons, and positrons and 0.1 GeV for muons and hadrons [126]

# Extensive air showers

The classical technique for the measurement of extensive air showers is the **sampling of shower particles at sea level with typically  $1 \text{ m}^2$  large scintillators or water Cherenkov counters**. This technique is sketched in Fig. 7.28.

In the **Auger project in Argentina** 1600 sampling detectors spread over an area of  $3000 \text{ km}^2$  will be used for the measurement of the ground-level component of extensive air showers. However, **the energy assignment for the primary particle using this technique is not very precise**. The shower develops in the atmosphere, which acts as a calorimeter of 27 radiation lengths thickness. The **information on this shower is sampled in only one, the last layer of this calorimeter and the coverage of this layer is on the order of much less than 1%**. The **direction of incidence of the primary particle can be obtained from the arrival times of shower particles in the different sampling counters (see Fig. 7.28)**.

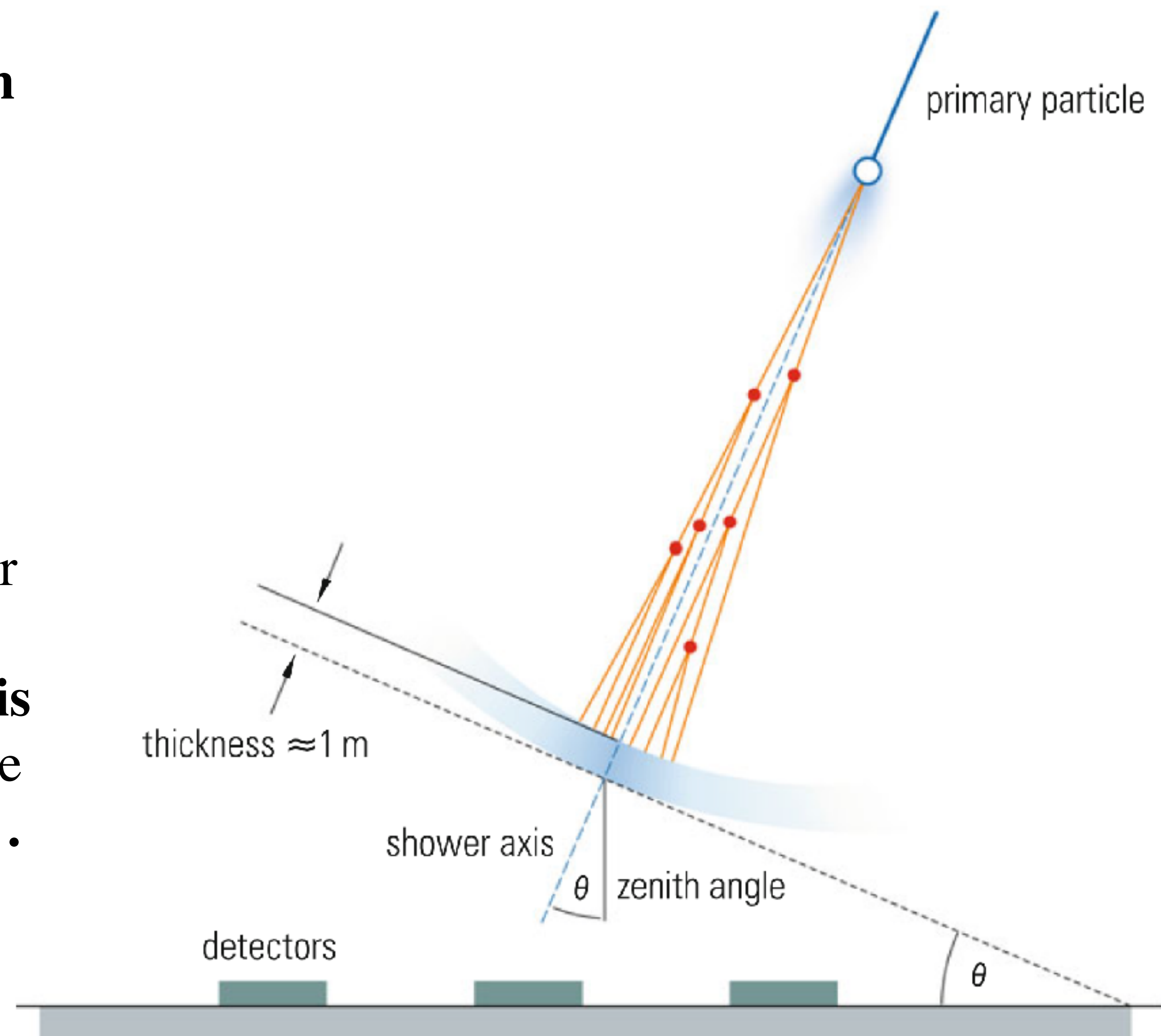
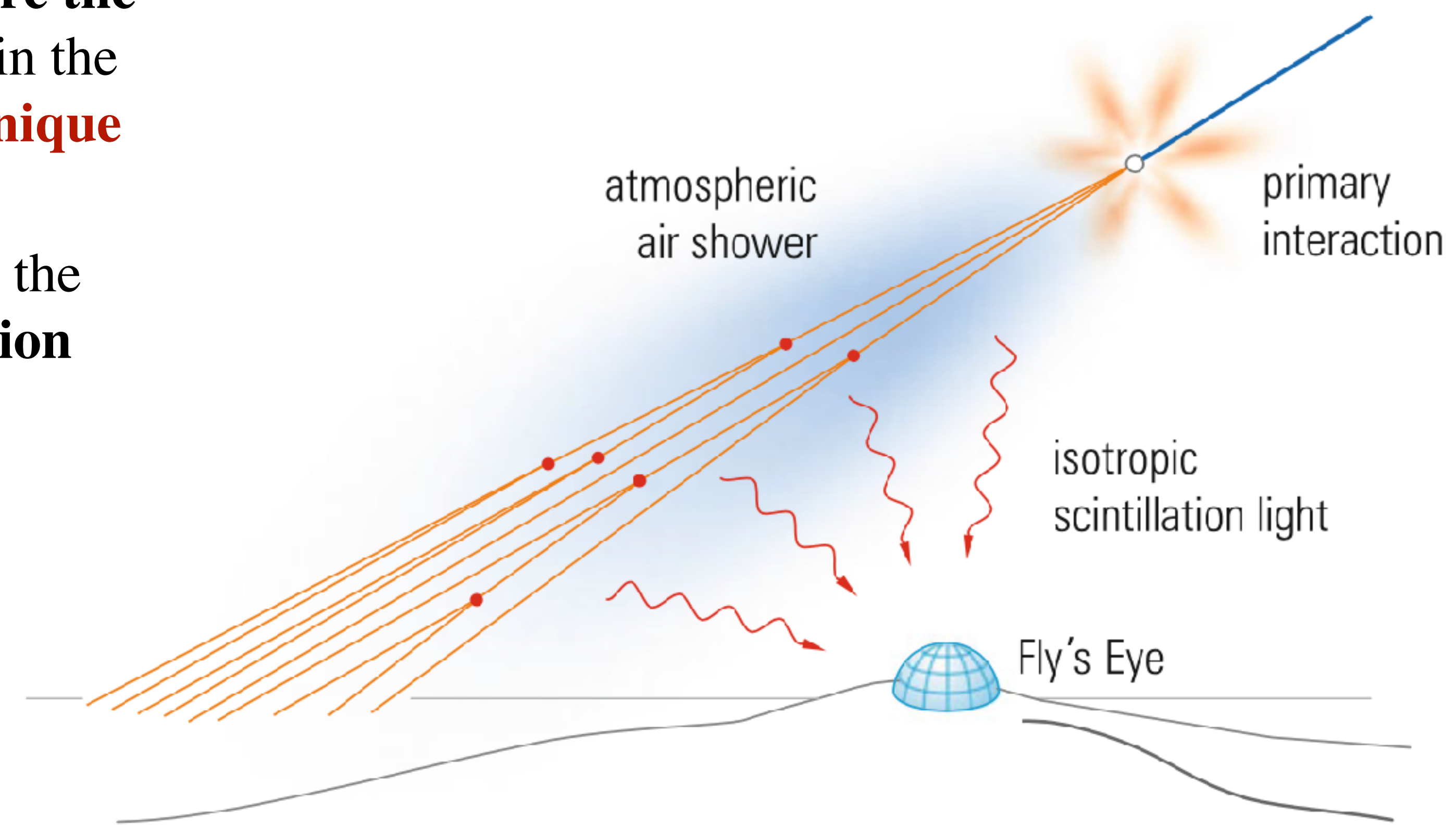


Fig. 7.28 Air-shower measurements with sampling detectors

# Extensive air showers

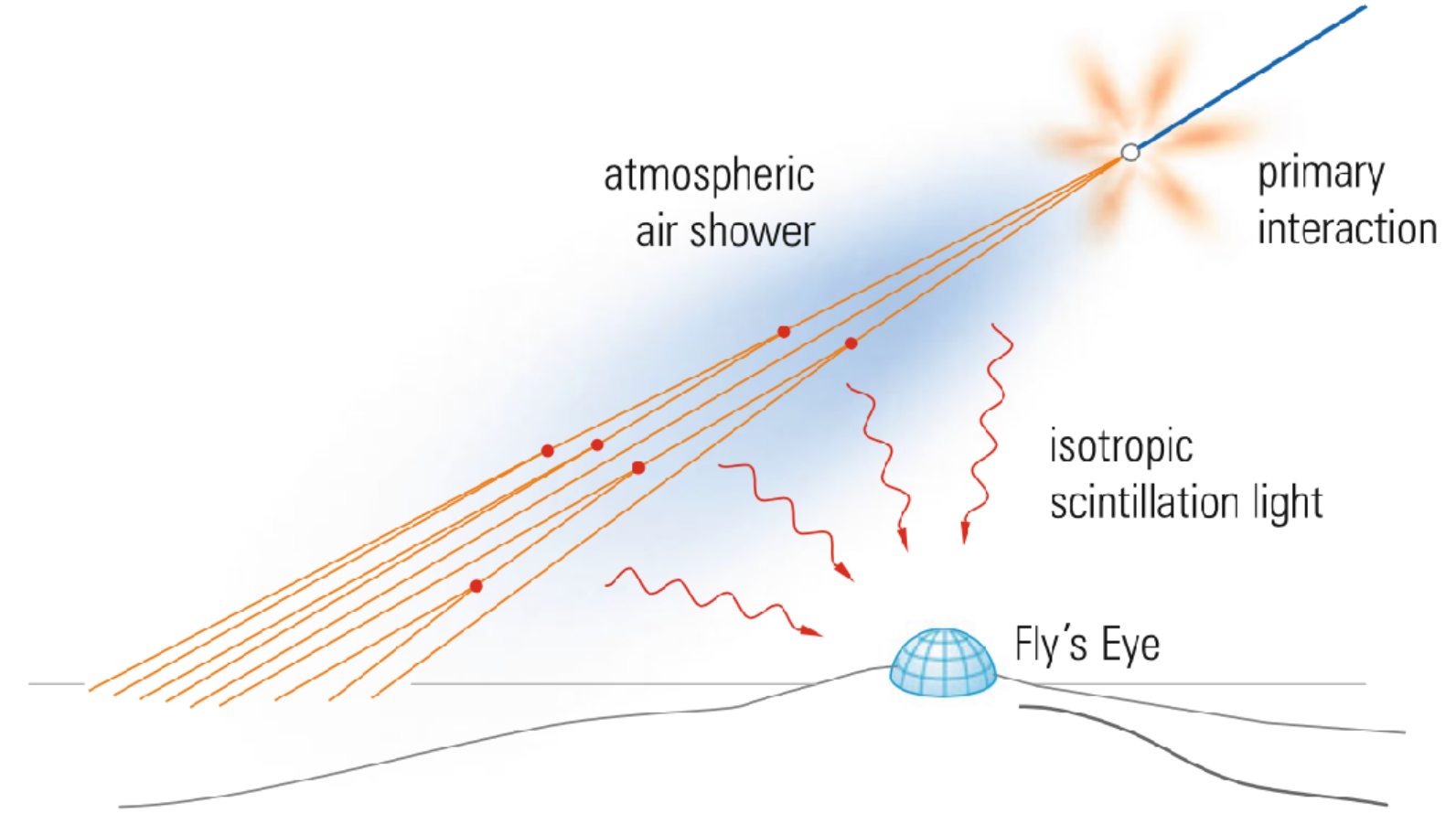
It would be much **more advantageous to measure the total longitudinal development of the cascade** in the atmosphere. This can be achieved using the **technique of the Fly's Eye** (Fig. 7.29).

Apart from the directional **Cherenkov radiation** the shower particles also emit **an isotropic scintillation light** in the atmosphere.



**Fig. 7.29** Principle of the measurement of scintillation light of extensive air showers

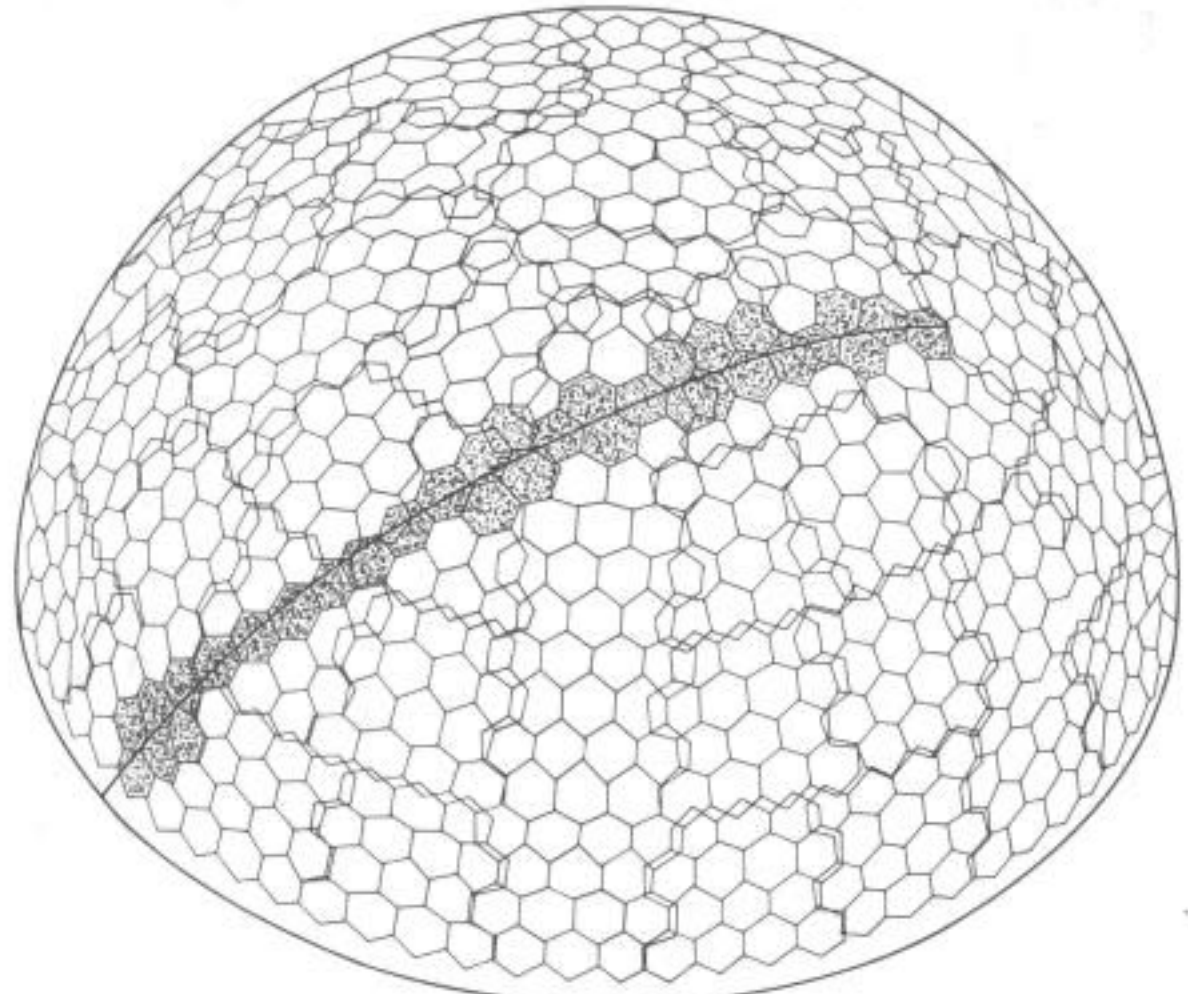
# Extensive air showers



## The Utah Fly's Eye experiment.

More information on how the detector worked: <http://www.telescopearray.org/index.php/history/the-fly-s-eye-1981-1993?showall=1&limitstart=1>

Fig. 7.29 Principle of the measurement of scintillation light of extensive air showers



# Extensive air showers

The *Auger experiment in Argentina* uses surface detectors and **fluorescence telescopes**, where the latter **record the longitudinal development of the air shower**.

Figures 7.30 and 7.31 show two examples of high-energy showers of  $2 \times 10^{18}$  eV respectively  $10^{19}$  eV energy, which develop their **shower maxima at different atmospheric depths**.

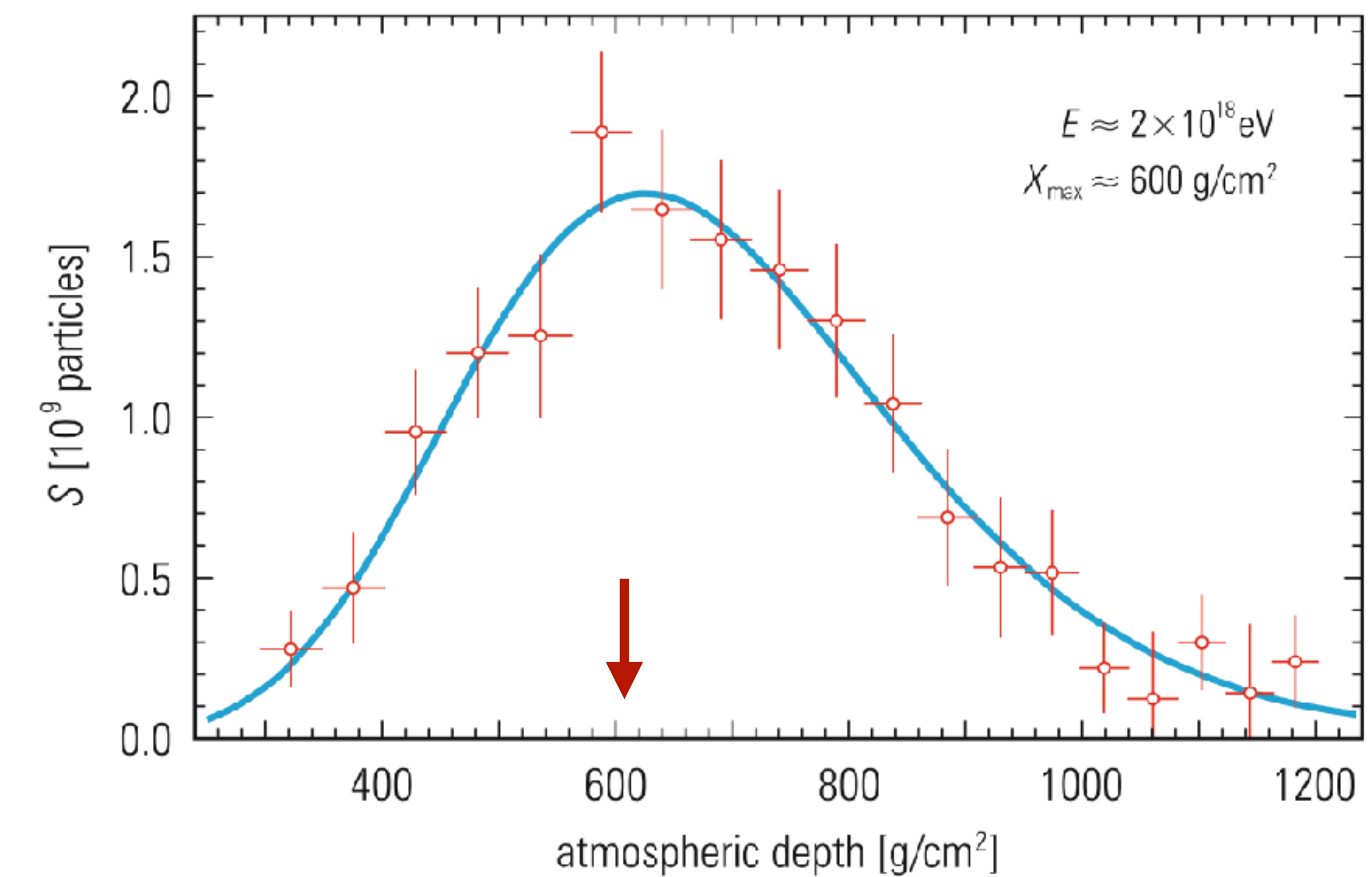


**Fig. 7.30** Measured longitudinal development of an air shower with energy  $2 \times 10^{18}$  eV in the Auger experiment. The depth of the shower maximum is at about  $600 \text{ g/cm}^2$  [127]

# Extensive air showers

The *Auger experiment in Argentina* uses surface detectors and **fluorescence telescopes**, where the latter **record the longitudinal development of the air shower**.

Figures 7.30 and 7.31 show two examples of high-energy showers of  $2 \times 10^{18}$  eV respectively  $10^{19}$  eV energy, which develop their **shower maxima at different atmospheric depths**.

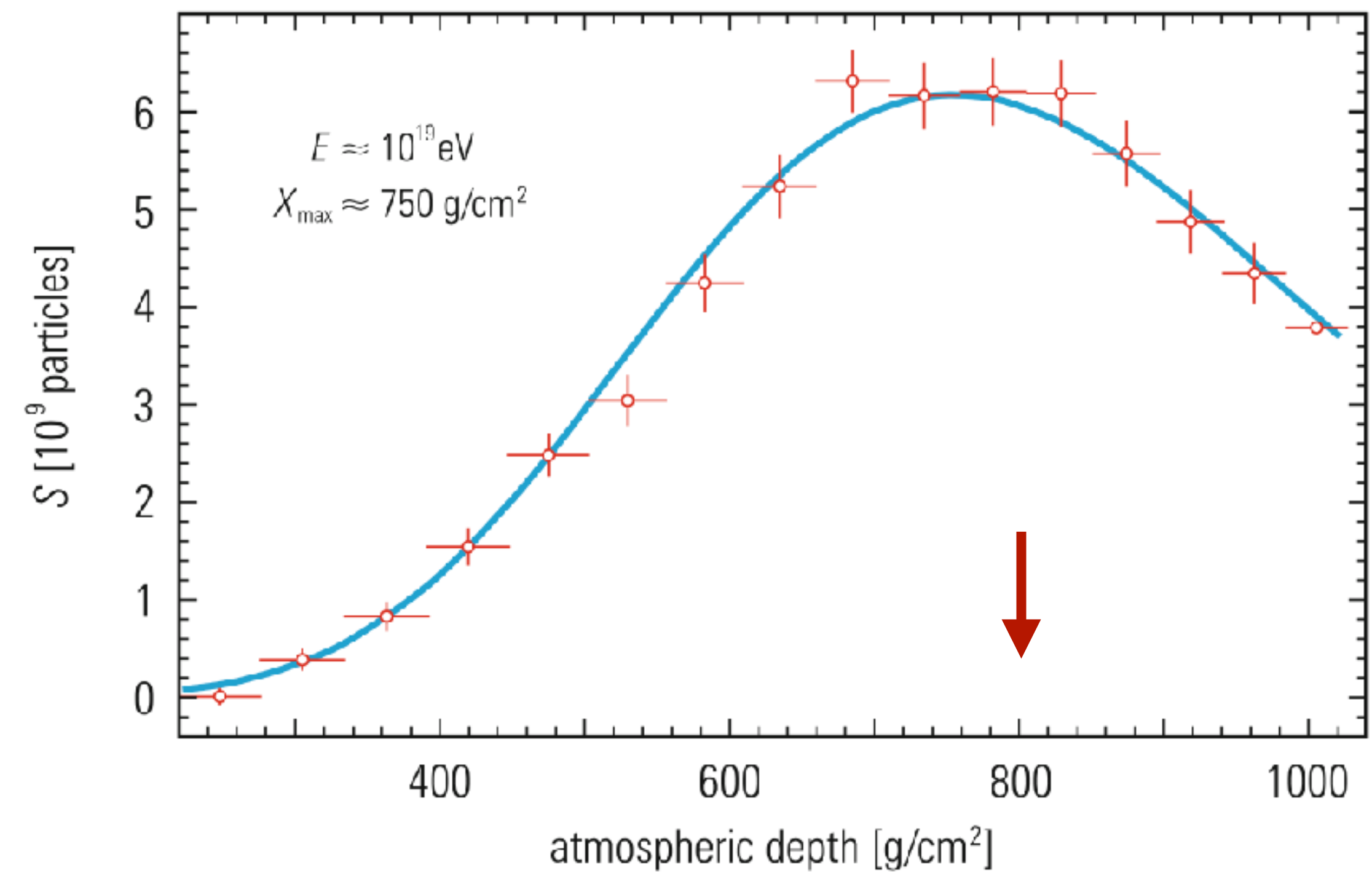


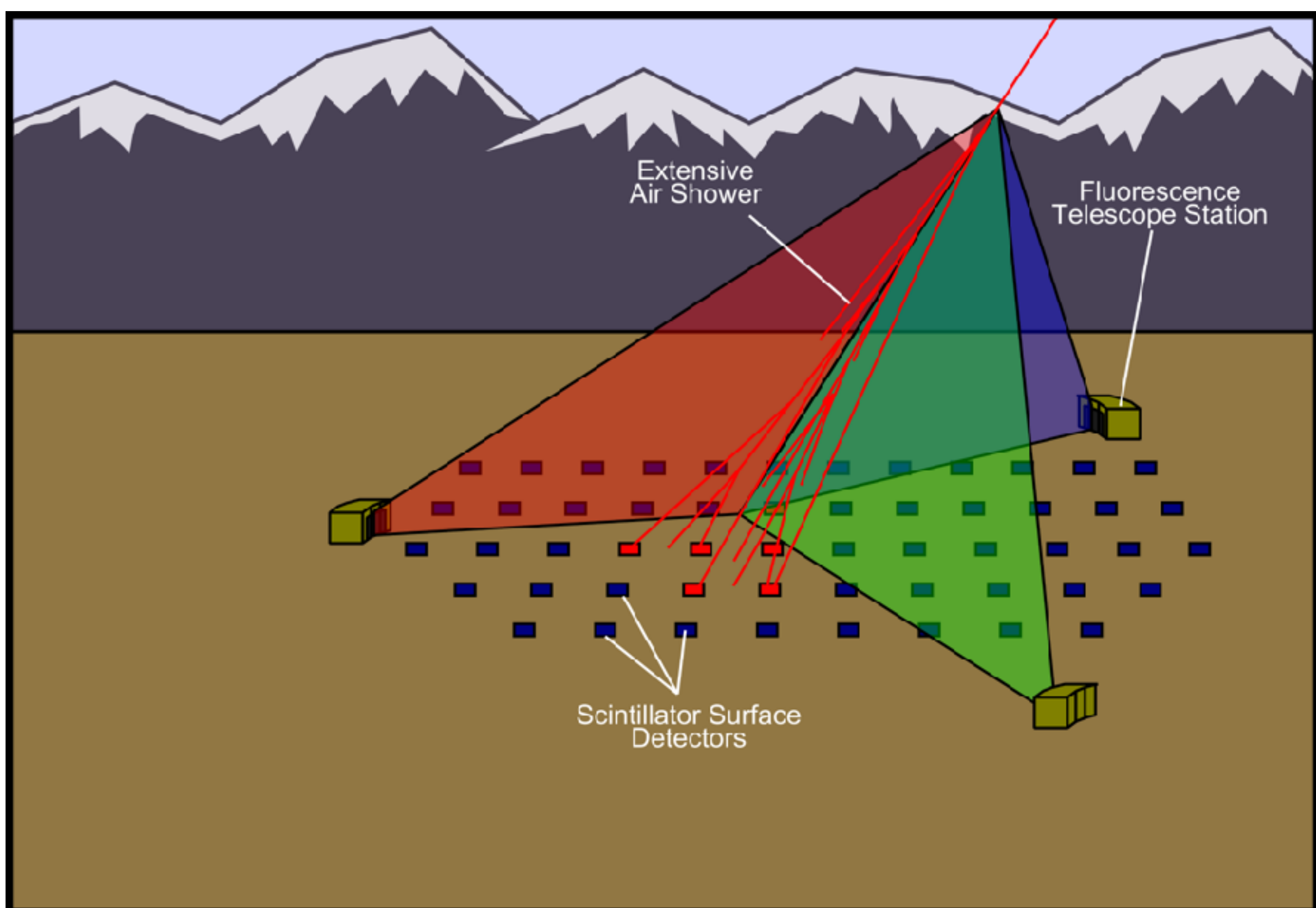
**Fig. 7.31** Measured longitudinal development of an air shower of energy  $10^{19}$  eV in the Auger experiment. The depth of the shower maximum is at around  $750 \text{ g/cm}^2$  [127]

# Extensive air showers

The energy domain covered by the Auger experiment is now also investigated by the **large Telescope Array (TA) in Millard County, Utah** (this is the successor of the Fly's Eye experiment).

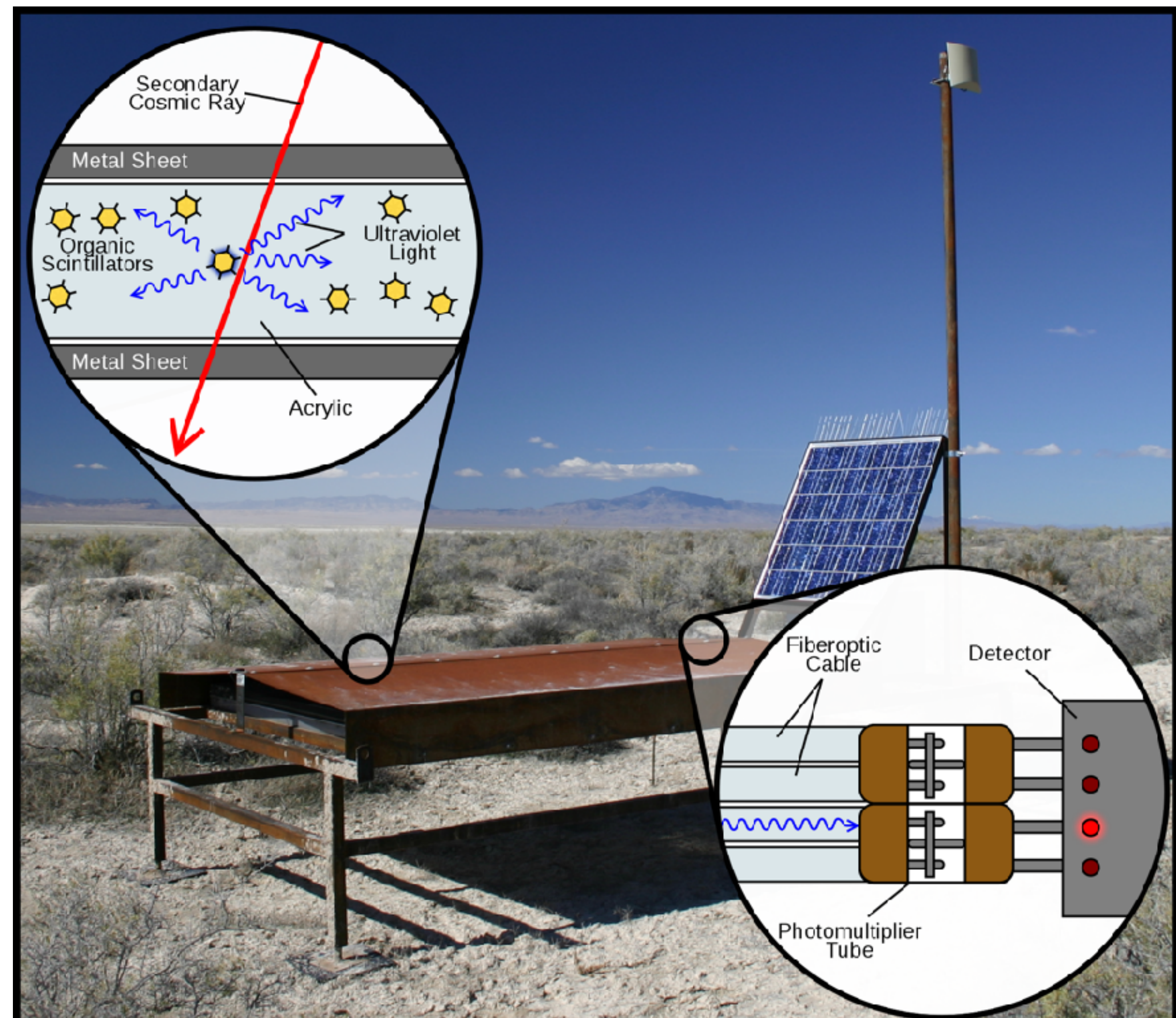
It also uses a ground array along with an air-fluorescence technique for the measurement of the highest cosmic-ray energies.

Data collection began in 2008.



# Extensive air showers

The ground array of the **large Telescope Array (TA)**. This is also a type of scintillation detector, but the scintillation happens inside of the detector and not in the atmosphere.



# Extensive air showers

For particles with **energies exceeding  $10^{17}$  eV** the fluorescence light of nitrogen is sufficiently intense to be recorded at sea level in the presence of the diffuse background of starlight. The actual detector consists of a system of **mirrors and photomultipliers**, which view the whole sky. An air shower passing through the atmosphere near such a Fly's Eye type detector activates only those photomultipliers whose field of view is hit. The fired photomultipliers **allow to reconstruct the longitudinal profile of the air shower**.

The **total recorded light intensity is used to determine the shower energy**. Such a type of detector allows much more precise energy assignments, however, it has a big **disadvantage** compared to the classical air-shower technique that it can **only be operated in clear moonless nights**.

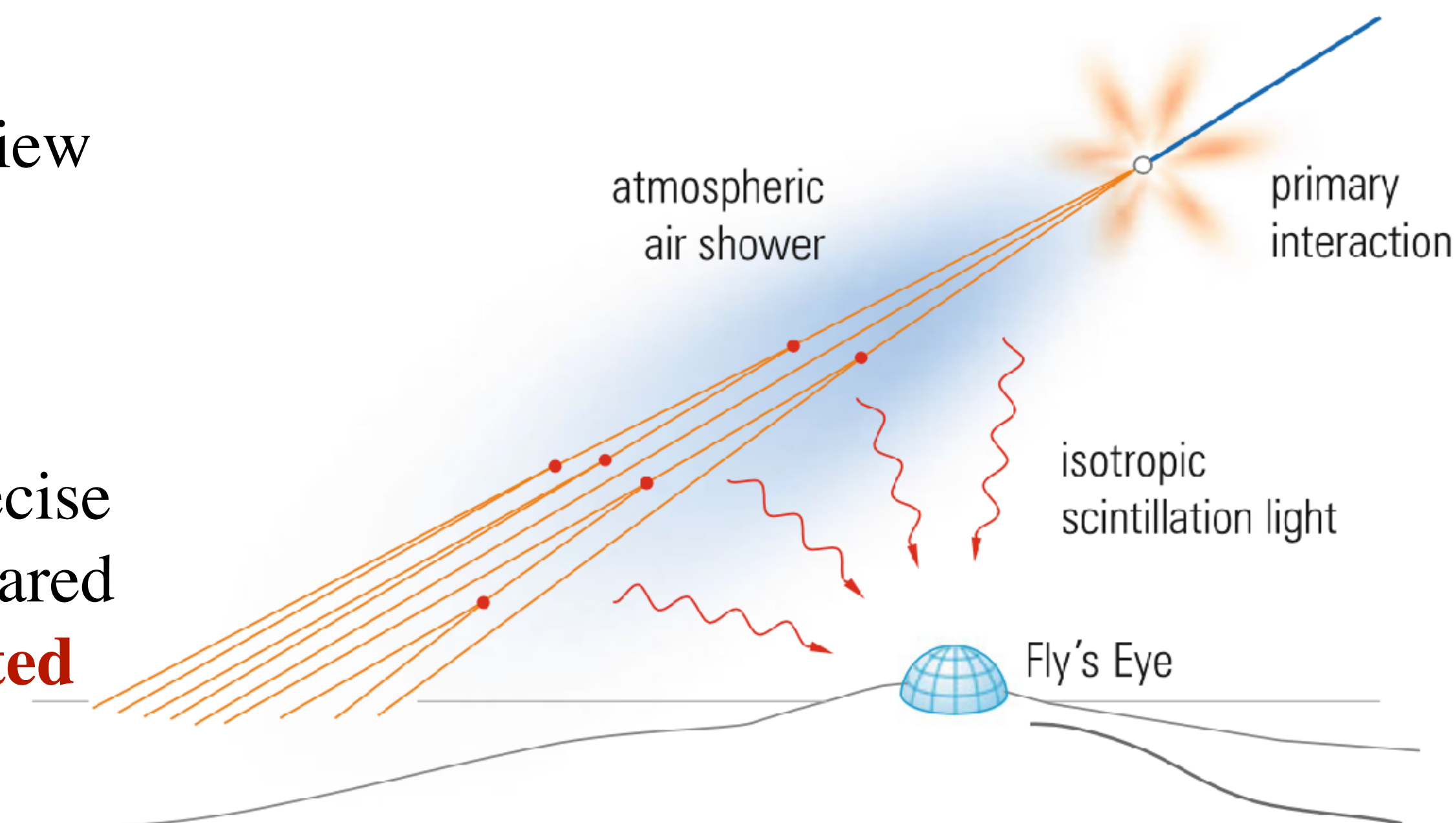
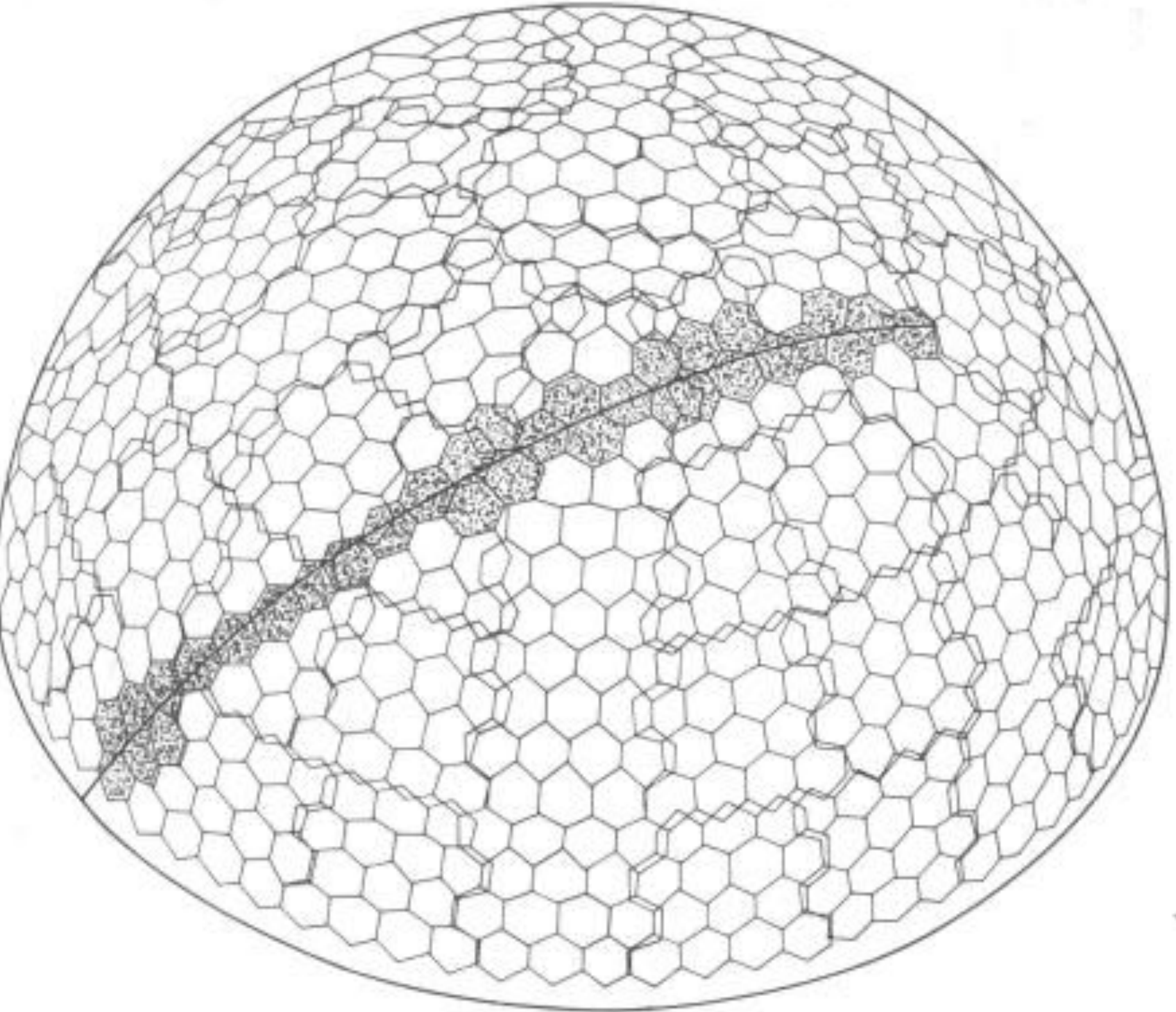


**Fig. 7.29** Principle of the measurement of scintillation light of extensive air showers

# Extensive air showers

The Utah Fly's Eye experiment.



Track of an air shower.

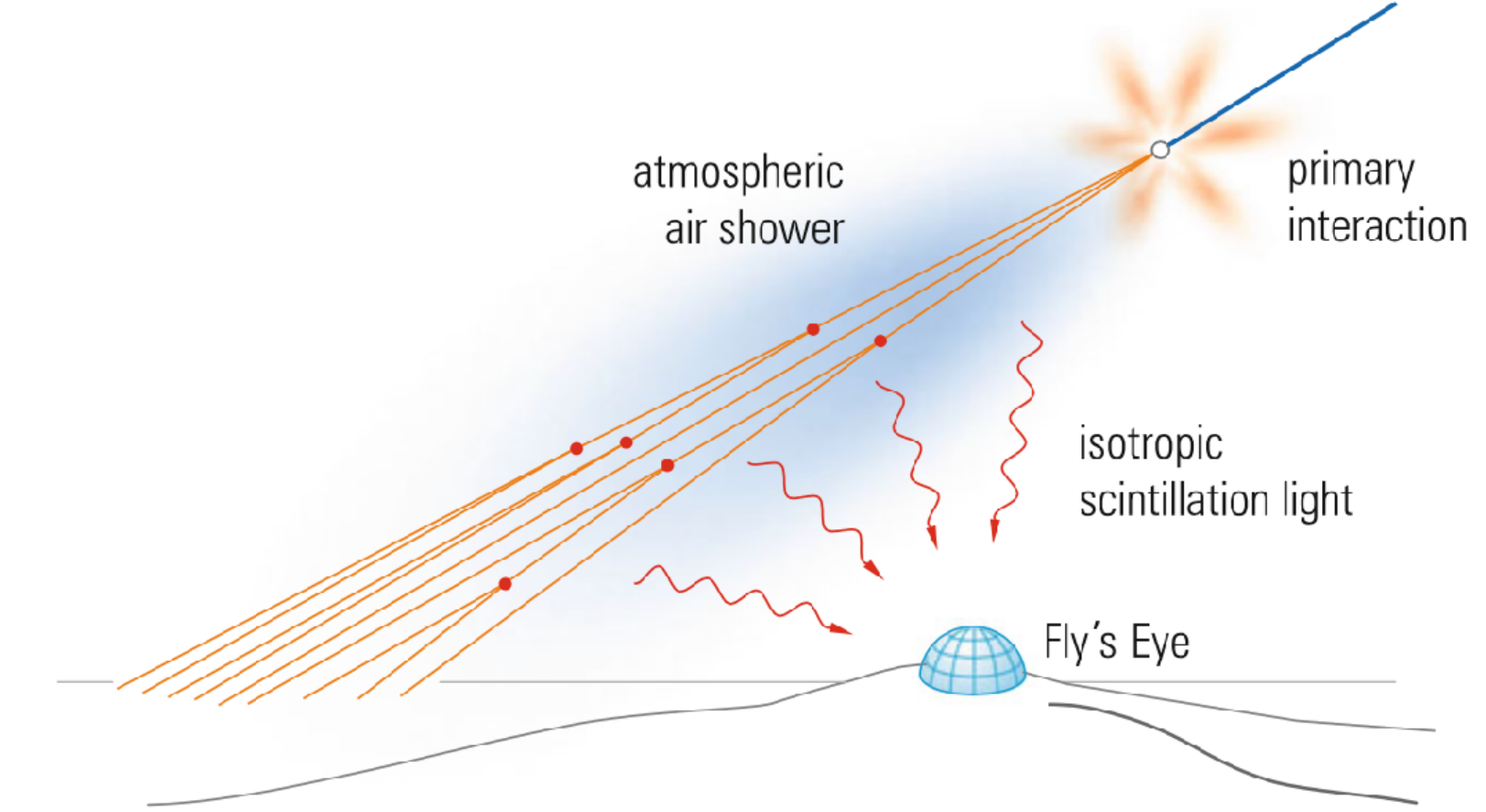
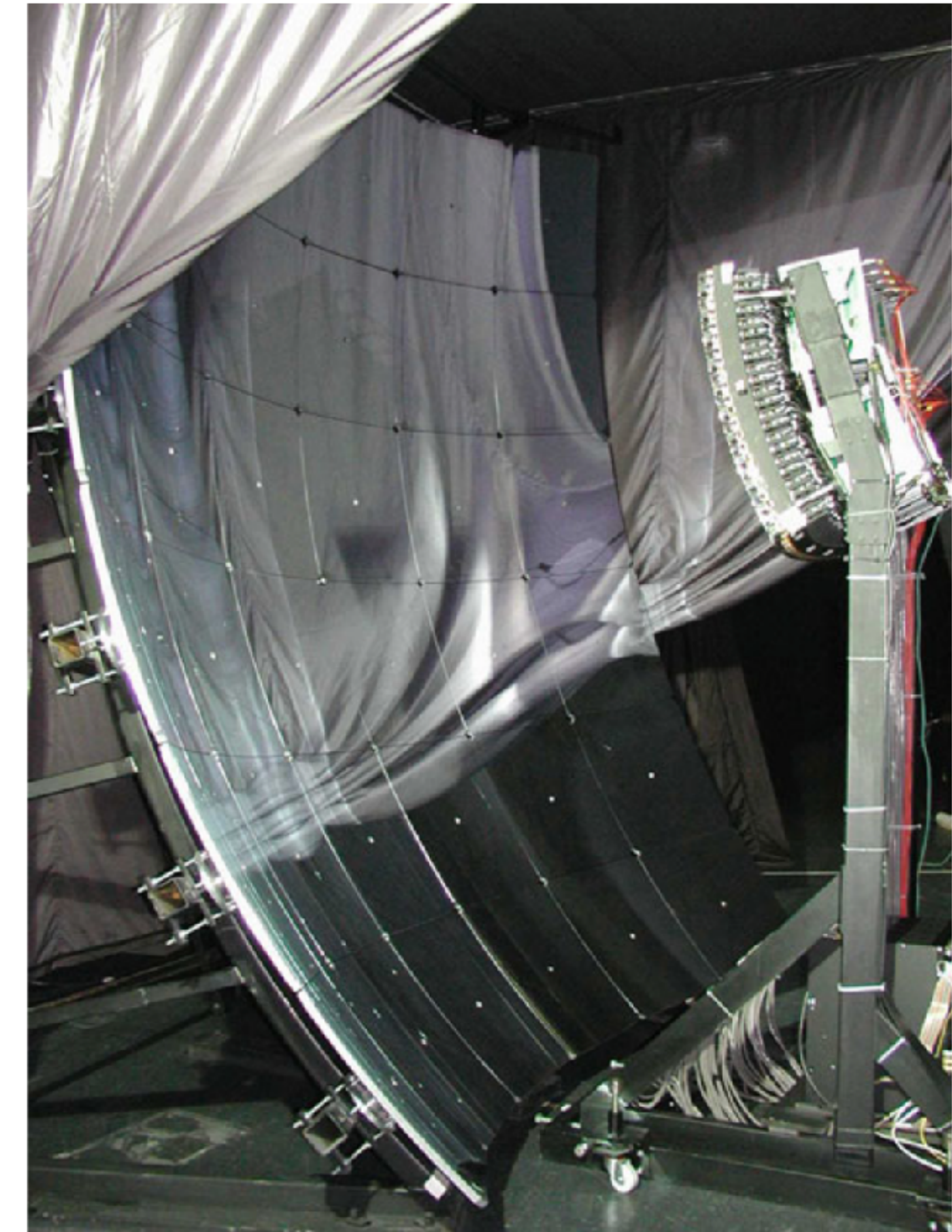


Fig. 7.29 Principle of the measurement of scintillation light of extensive air showers



# Extensive air showers

In the **Auger experiment** the array of sampling detectors is complemented by a number of telescopes, which measure the scintillation light produced in the atmosphere. Figure 7.32 shows one of the mirrors of the Auger telescopes along with its camera of photomultipliers mounted in its focal point.



**Fig. 7.32** Photo of a mirror and camera of a detector for the measurement of fluorescence radiation in the Auger experiment [129]

# Extensive air showers

Much larger acceptances could be provided if such a **Fly's Eye type detector would be installed in orbit**. There is in fact a proposal to observe air showers from space. Such an experiment would **record the air showers from a detector at the ISS in the Earth's orbit (JEM- EUSO)**, see Fig. 7.33.

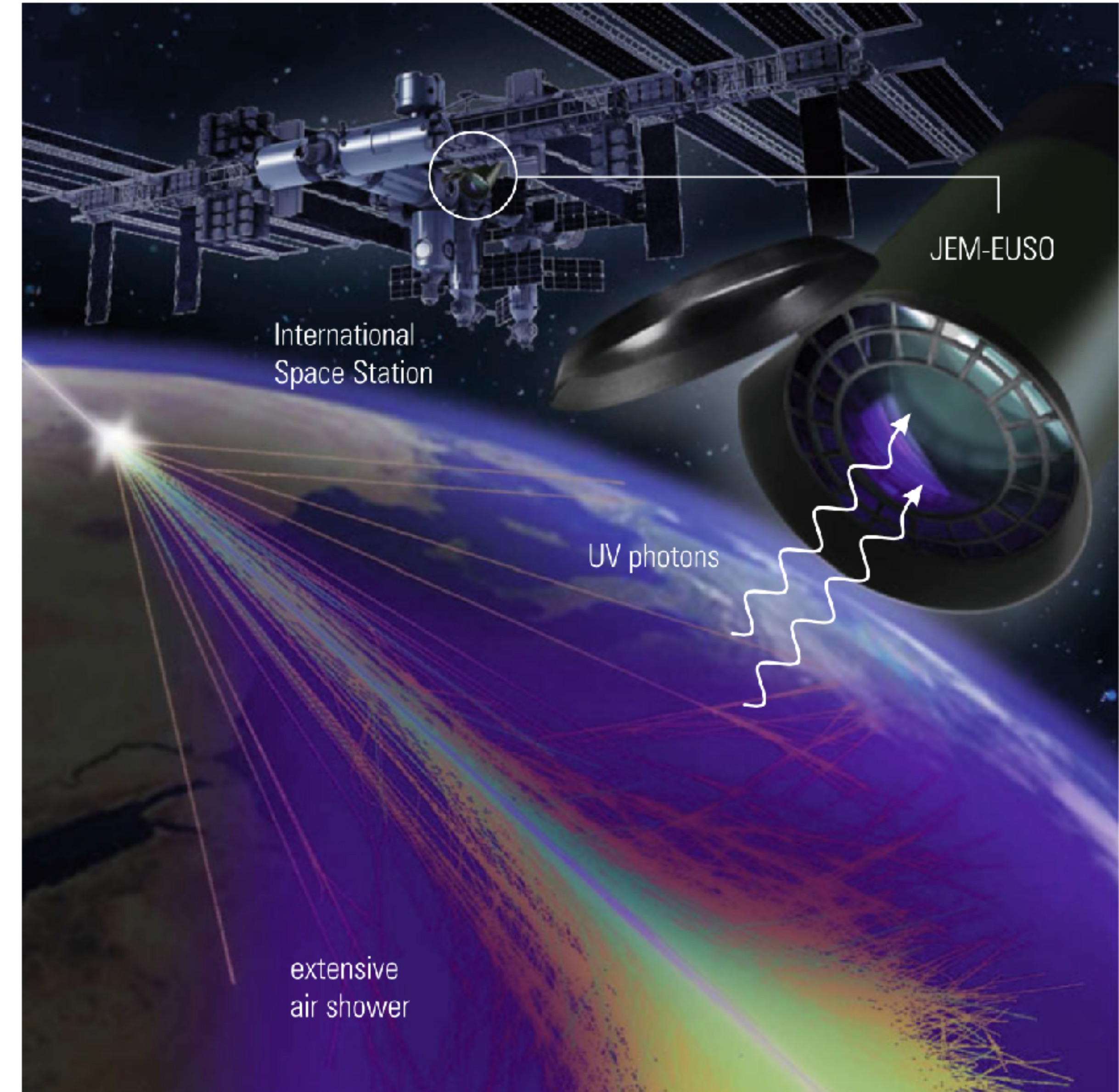


**Fig. 7.33** Proposal for an experiment for the observation of air showers from an experiment in the Earth's orbit (JEM-EUSO; Extreme Universe Space Observatory in the Japanese module of the International Space Station) at the ISS [130]

# Extensive air showers

As a result of the **different detection techniques**, Fig. 7.34 shows the **measured all-particle spectrum of primary cosmic rays**.

## Detection technics:

- scintillation light
- Water Cherenkov
- Radio detection
- Acoustic detection
- Underground muon detectors

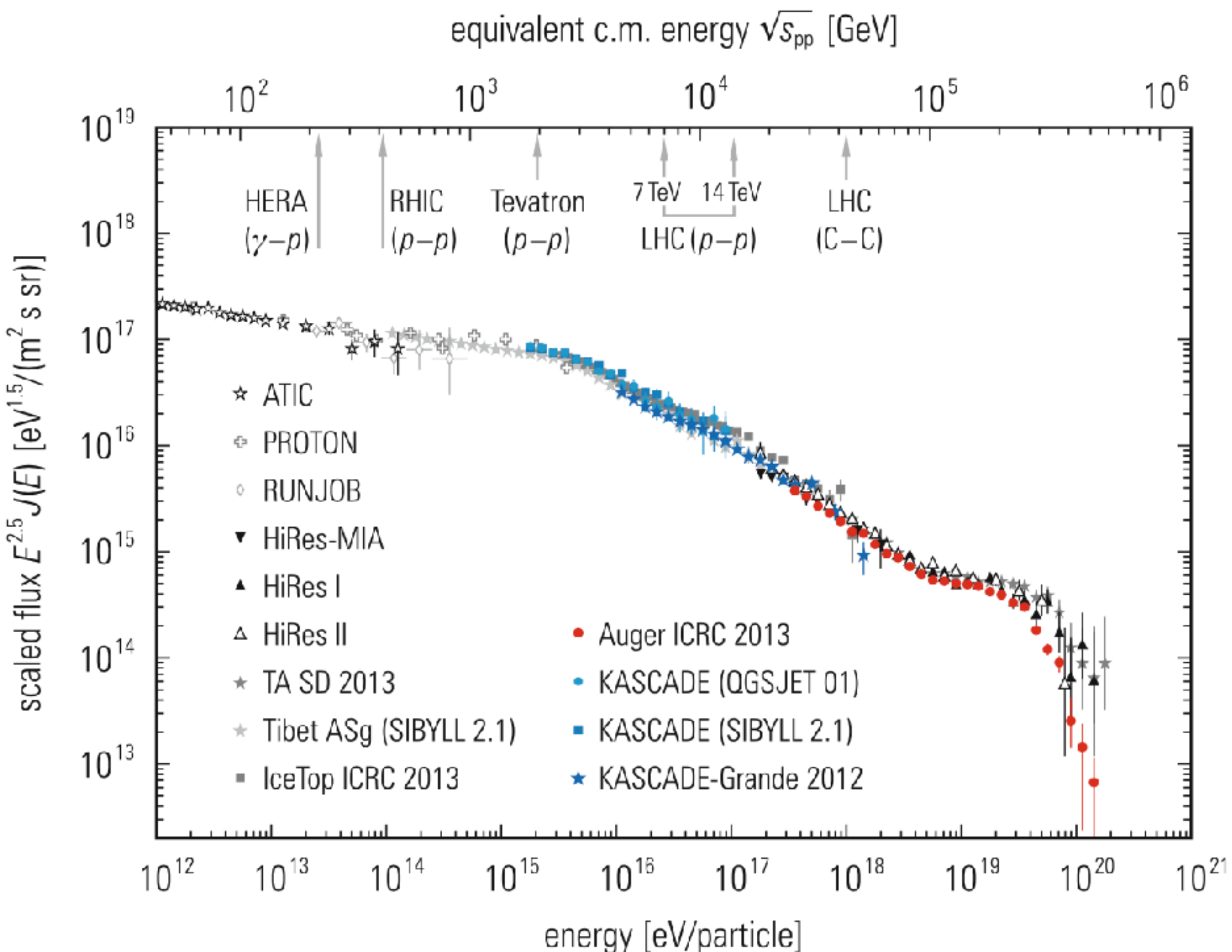


**Fig. 7.34** All-particle spectrum of primary cosmic rays. The scatter at very high energies also shows the problems of an accurate energy assignment [131, 132]

# Extensive air showers

It has been tried to observe air showers via the **electromagnetic radiation emitted in the radio band**. It is generally believed that this radio signal is caused by **shower electrons deflected in the Earth's magnetic field thereby creating synchrotron radiation**. In spite of the strong background in practically all wavelength ranges these attempts have been **quite successful, in particular, in the radio band from 40 to 80 MHz**.

The possibility to detect large air showers via their **muon content in underground experiments—possibly jointly with an air-shower detector on the surface in coincidence**—has been followed up in recent experiments.

A more exotic technique would be the **detection of the acoustic signal produced by high-energy particles in water or ice** (see also Sect. 7.6: ‘Acoustic Detection of Air Showers’).

# Extensive air showers

## Goals:

- measuring chemical composition
- Measuring the energy of the primary
- Identifying the acceleration sites

Apart from elementary-particle-physics aspects the purpose of the measurement of extensive air showers is the **determination of the chemical composition of primary cosmic rays** and the search for the **sites of cosmic accelerators**.

Both of these problems are hard to solve. The **chemical composition up to the TeV range can be determined with balloons or satellites in direct measurements**, but beyond that one has to resort to extensive air showers. The determination of the mass of a primary cosmic-ray particle with **energy  $>10^{15}$  eV** is very **indirect**.

The **position of the shower maximum or the muon content** of an air shower provides some evidence of the **nature of the primary particle** that has initiated the shower.

# Extensive air showers

Figure 7.35 gives an idea of the problem: The **mean logarithmic mass is plotted against the primary energy**.

There are indications that the **masses of the primary cosmic rays get heavier beyond the knee** ( $\approx$  several PeV). At the **highest energies lighter particles seem to be dominant**.

From the inspection of the figure one can appreciate that **it is obviously not easy to determine the mass of a particle whose energy is more than a million times heavier than its rest mass**. The scatter of the experimental results is substantial.

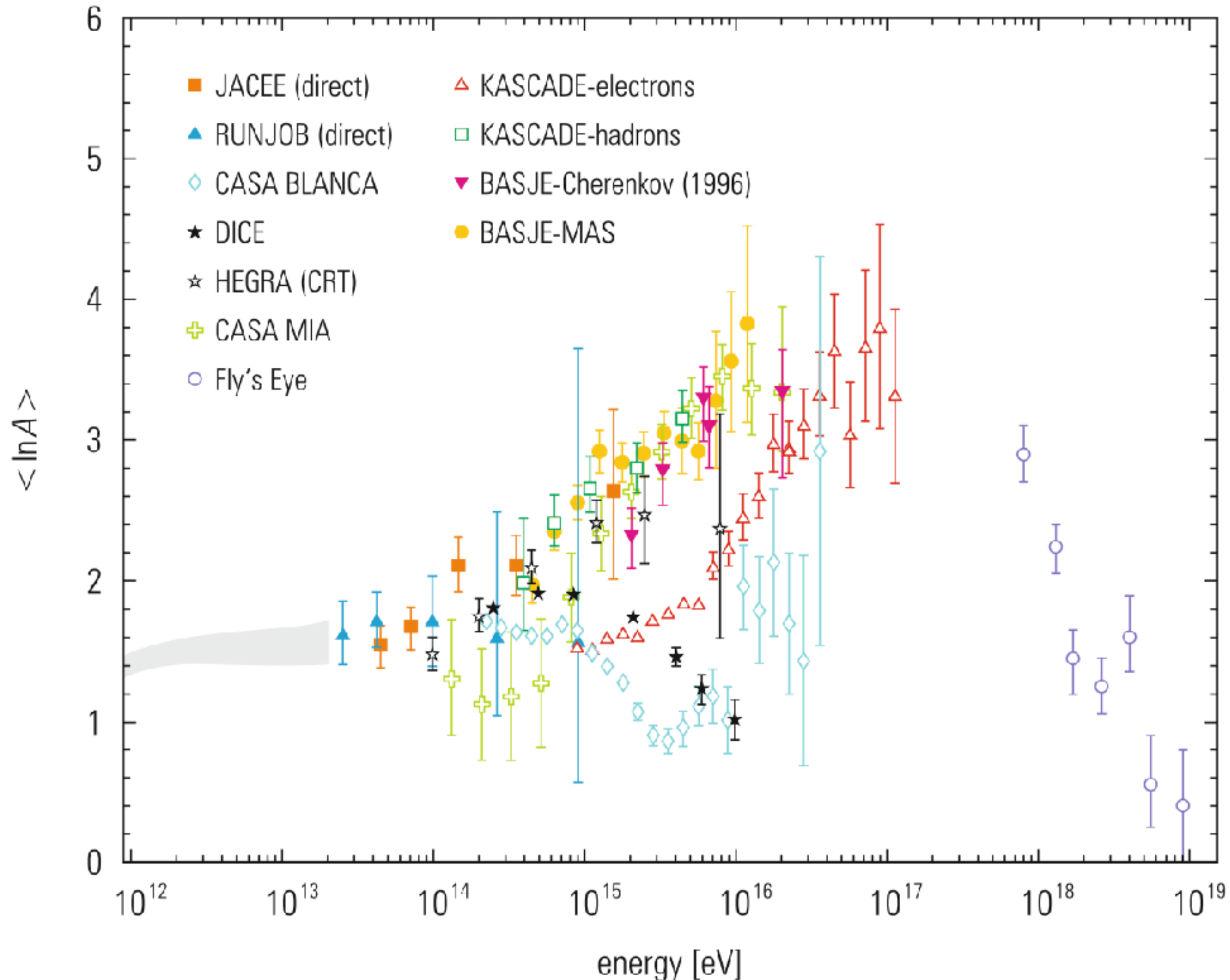


Fig. 7.35 Mean logarithmic mass  $\langle \ln A \rangle$  for primary cosmic rays for high energies [132]

# Extensive air showers

The arrival directions of the **highest-energy particles ( $>10^{19}$  eV)**, practically show **no correlation to the galactic plane**. This clearly indicates that their origin **must be extragalactic**.

If the highest-energy primary cosmic-ray particles are **protons**, then their **energies must be below  $10^{20}$  eV, if they originate from distances of more than 50Mpc**. Even if their original energy were much higher, they would **lose energy by photoproduction of pions** (Greisen–Zatsepin–Kuzmin cutoff ( $\approx 6 \times 10^{19}$  eV)). Protons of this energy would **point back to the sources**, because galactic and intergalactic magnetic fields only cause angular distortions on the order of one degree at these high energies.

The irregularities of **magnetic fields, however, could lead to significant time delays between  $\nu$  and  $\gamma$  and protons**, from such distant sources. This comes about because the **proton trajectories are somewhat longer, even though their magnetic deflection is rather small**. Depending on the distance from the source, **time delays of months and even years can occur for protons**.

This effect is of particular importance, if  $\gamma$ -ray bursters are also able to accelerate the highest-energy particles and if one wants to **correlate the arrival times of photons from  $\gamma$ -ray bursts with those of extensive air showers initiated by charged primaries**.

# Extensive air showers

Out of the up to now 27 measured highest-energy showers ( $>57$  EeV) in the Auger experiment one might see a **tentative evidence of a clustering along the supergalactic plane** (see Fig. 7.36).

The supergalactic plane is a **sheet-like structure containing the Local Supercluster, the Virgo Cluster, the Great Attractor, the Coma Supercluster, the Perseus–Pisces Supercluster, and the Shapley Concentration**.

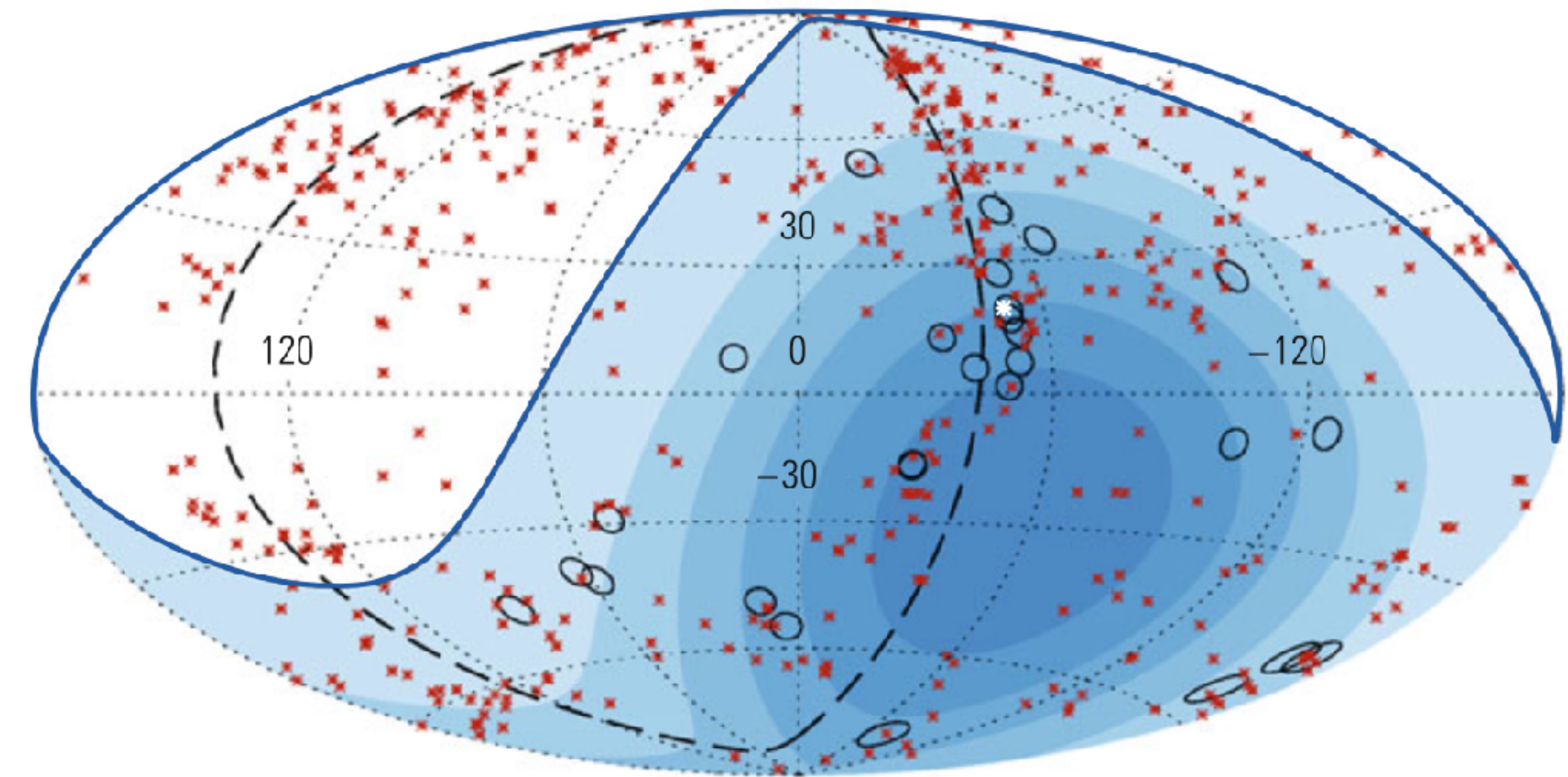
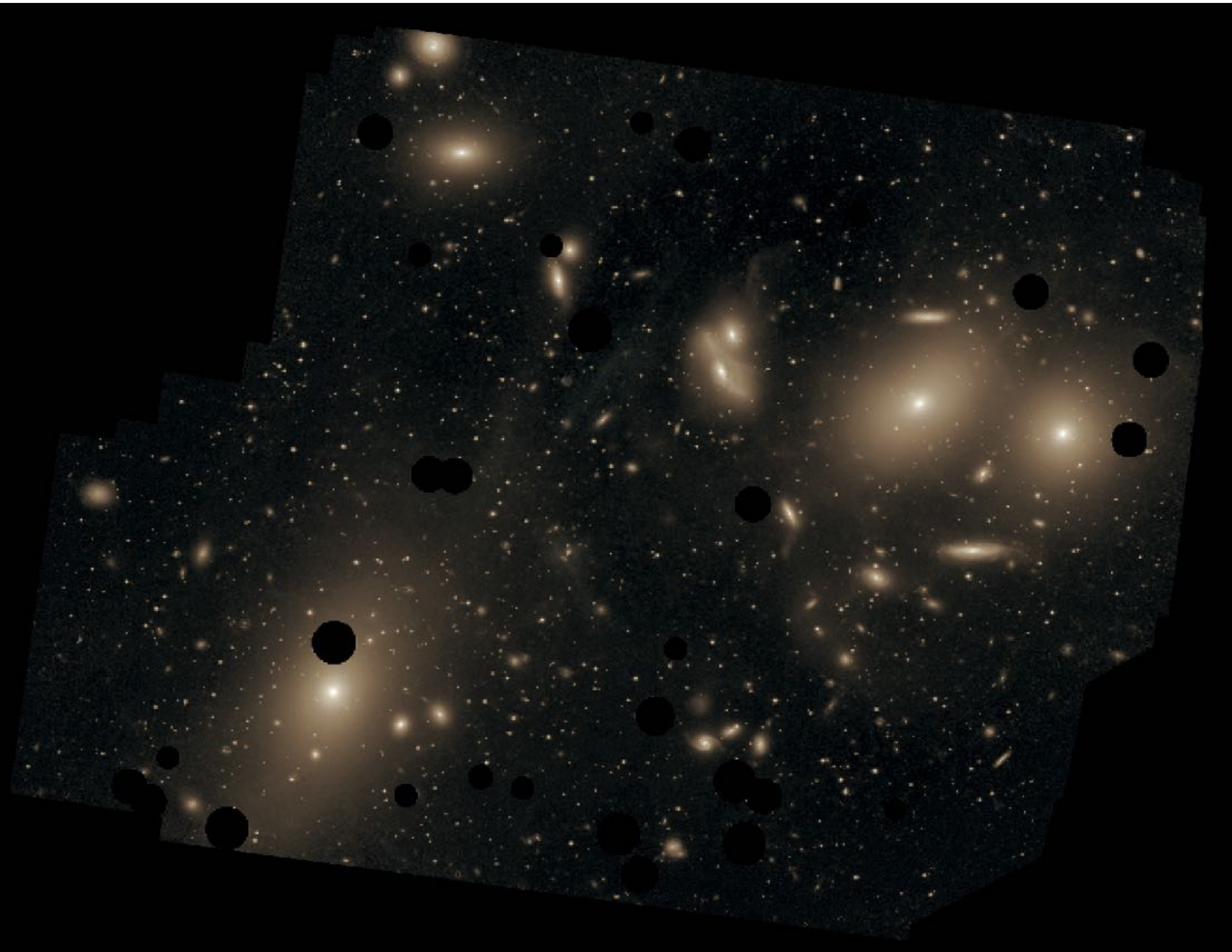


**Fig. 7.36** Arrival directions of the 27 most energetic air showers measured from the Auger experiment in galactic coordinates. The energies of the air showers are larger than 57 EeV. They are shown as open circles. At the same time the positions of 471 active galactic nuclei (AGNs) within 75 Mpc are given as *red stars* \*. The *blue region* defines—depending on the exposure time—the field of view of the Auger experiment. The *full line* shows the limit of the Auger acceptance. Centaurus A is marked as *white star* (\*). Two out of the 27 air-shower events arrive within the angular resolution of Auger from this direction. The *dashed line* indicates the position of the supergalactic plane [133]

# Extensive air showers

The Virgo galaxy Cluster is the closest galaxy cluster to us



# Extensive air showers

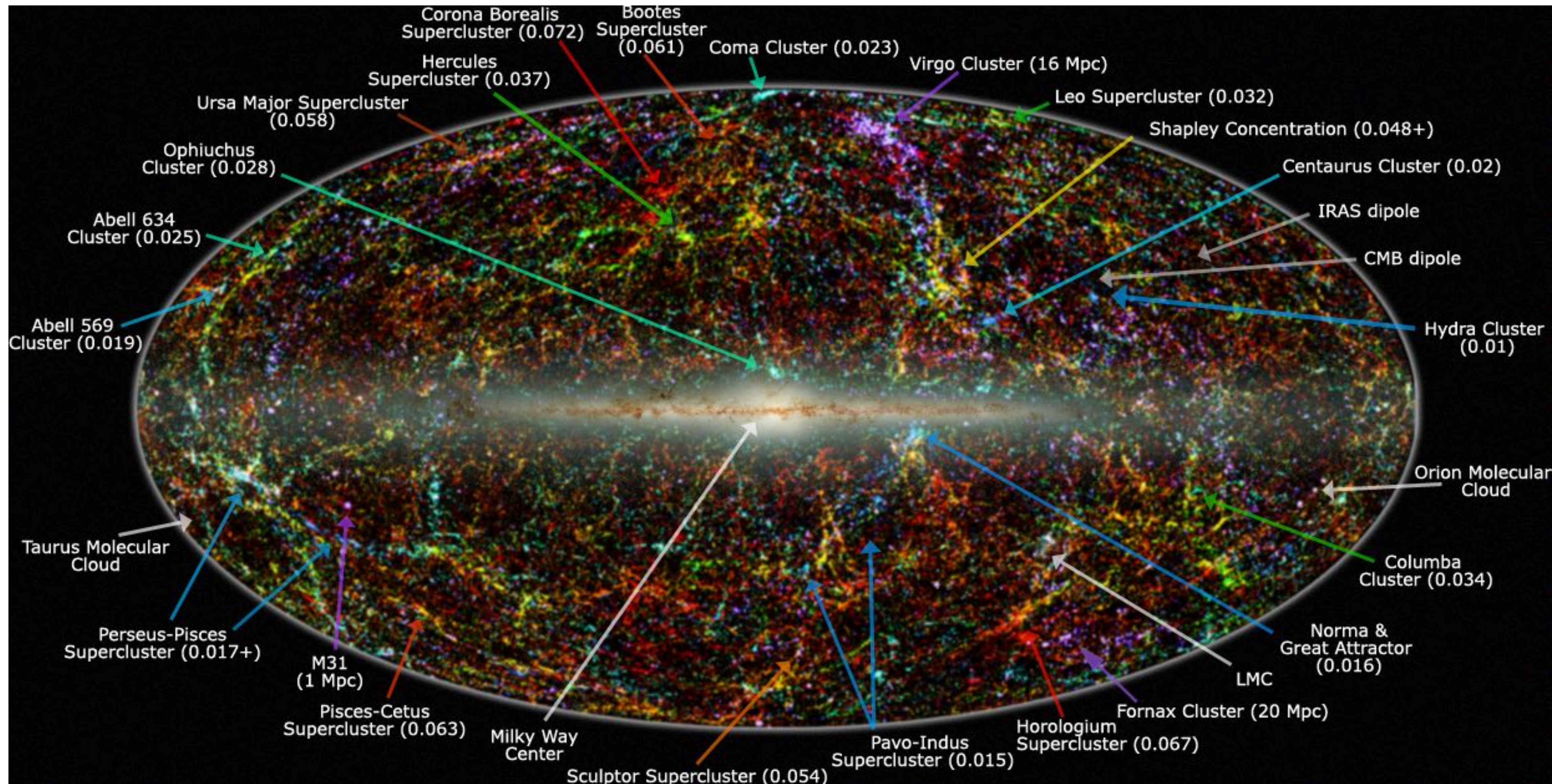
The Coma galaxy cluster



# Extensive air showers

Large scale structure

Each coloured point is a galaxy + the Milky Way



# Extensive air showers

**Two air-shower events** arrive within the experimental angular resolution of Auger from the **potential source Centaurus A** (white star in Fig.).

A correlation with active galactic nuclei observed in  $\gamma$  rays is not visible. **Better statistics are required.** Astronomy with a handful of events is not really possible. The latest news from Auger do not improve the statistical evidence for showers coming from Centaurus A.

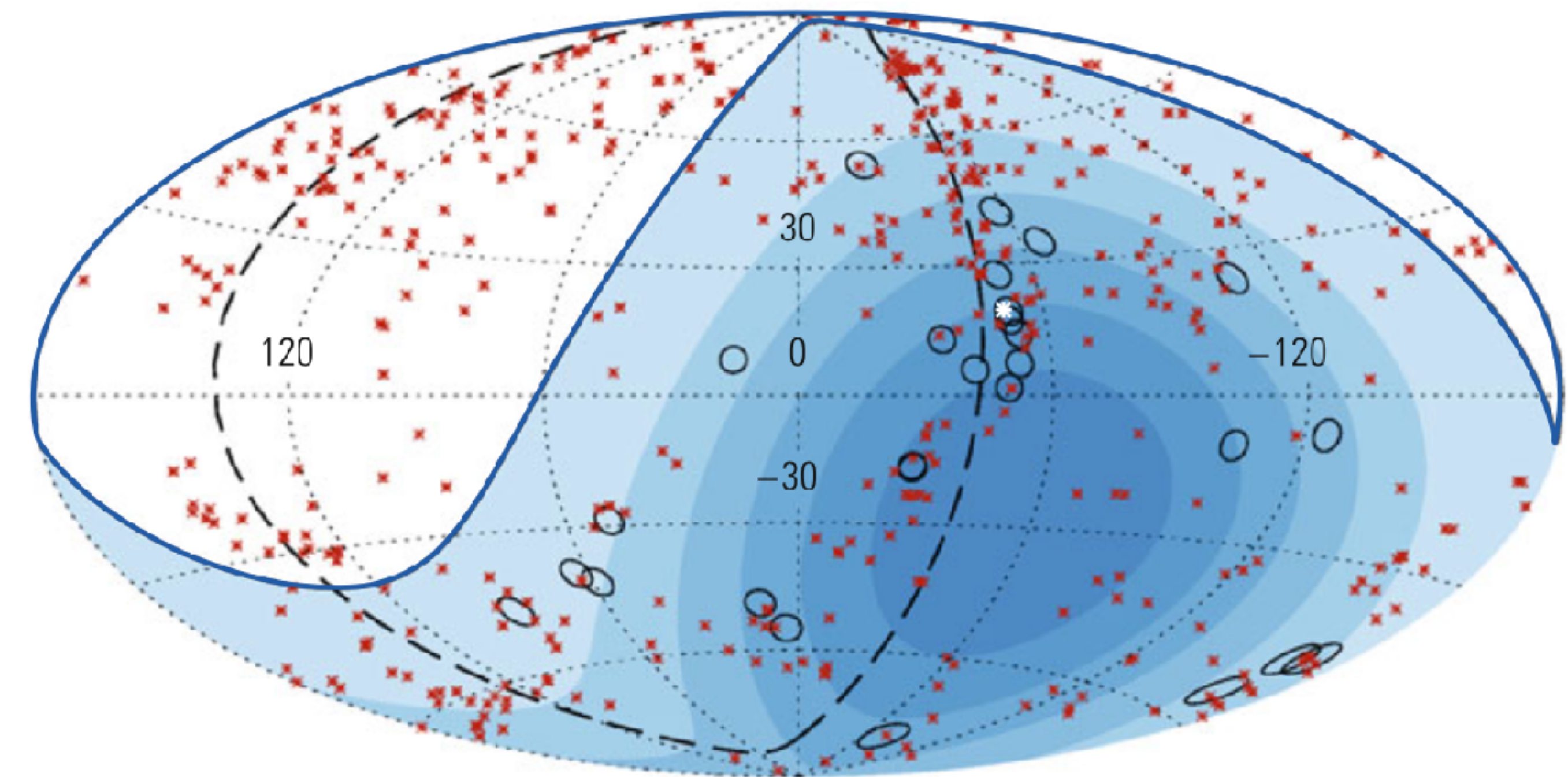
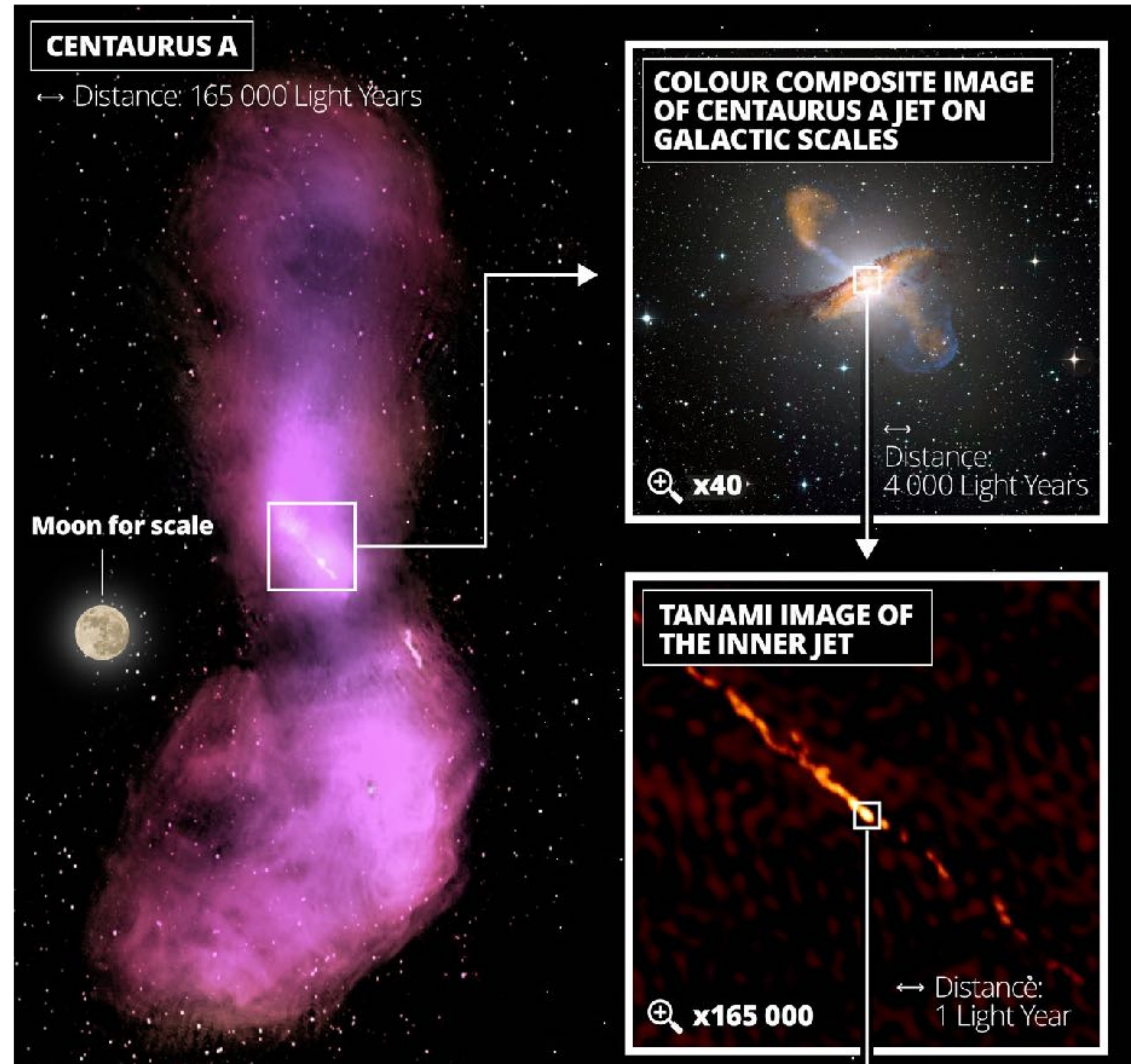


**Fig. 7.36** Arrival directions of the 27 most energetic air showers measured from the Auger experiment in galactic coordinates. The energies of the air showers are larger than 57 EeV. They are shown as open circles. At the same time the positions of 471 active galactic nuclei (AGNs) within 75 Mpc are given as *red stars* \*. The *blue region* defines—depending on the exposure time—the field of view of the Auger experiment. The *full line* shows the limit of the Auger acceptance. Centaurus A is marked as *white star* (\*). Two out of the 27 air-shower events arrive within the angular resolution of Auger from this direction. The *dashed line* indicates the position of the supergalactic plane [133]

# Extensive air showers

Centaurus A is one of the closest AGN at a distance of 3-5 Mpc, which is well within the GZK cutoff of 50 Mpc.



# Extensive air showers

However, recently the Auger experiment has observed a significant ( $5.2\sigma$ ) **large-scale dipole anisotropy for showers of energy above  $8 \times 10^{18}$  eV.**

Figure 7.37 shows the fluxes of high-energy particles in galactic coordinates. The galactic center is at the origin. The cross indicates the measured dipole direction; the contours denote the 68% and 95% confidence-level regions. The direction of the dipole anisotropy shown in the figure is assumed to be **correlated with mass aggregations and centers of possible sites of acceleration**. The position of the dipole anisotropy for the highest-energy primary particles indicates an **extragalactic origin for these events**.

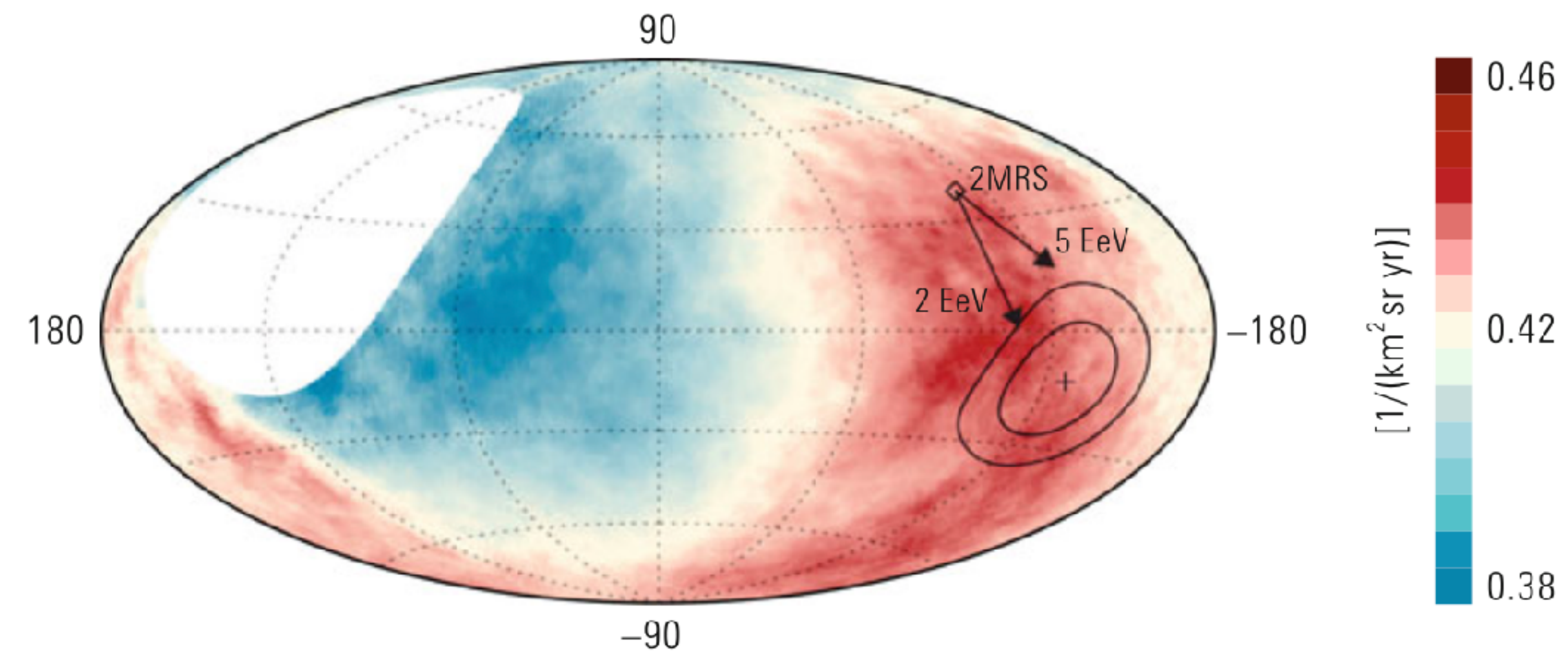


**Fig. 7.37** Auger sky map in galactic coordinates showing the cosmic-ray flux for energies in excess of 8 EeV. The direction of the dipole anisotropy indicates an extragalactic origin for these ultra-high-energy particles. The direction of the dipole anisotropy observed with the near-infrared flux of photons (the 2 Micron all-sky Redshift Survey (2MRS)) is indicated. The arrows show the expected deflections of particles with  $E/Z = 5$  EeV or 2 EeV from a possible origin in the 2MRS direction for a given typical galactic magnetic field [134]

# Extensive air showers

Normal extensive air showers have **lateral widths of at most 10 km**, even at the highest energies. However, there are indications that *correlations between arrival times of air showers over distances of more than 100km exist.*

Such coincidences could be understood by assuming that energetic **primary cosmic particles undergo interactions or fragmentations at large distances from Earth**. The **secondary particles produced in these interactions would initiate separate air showers in the atmosphere** (Fig. 7.38).

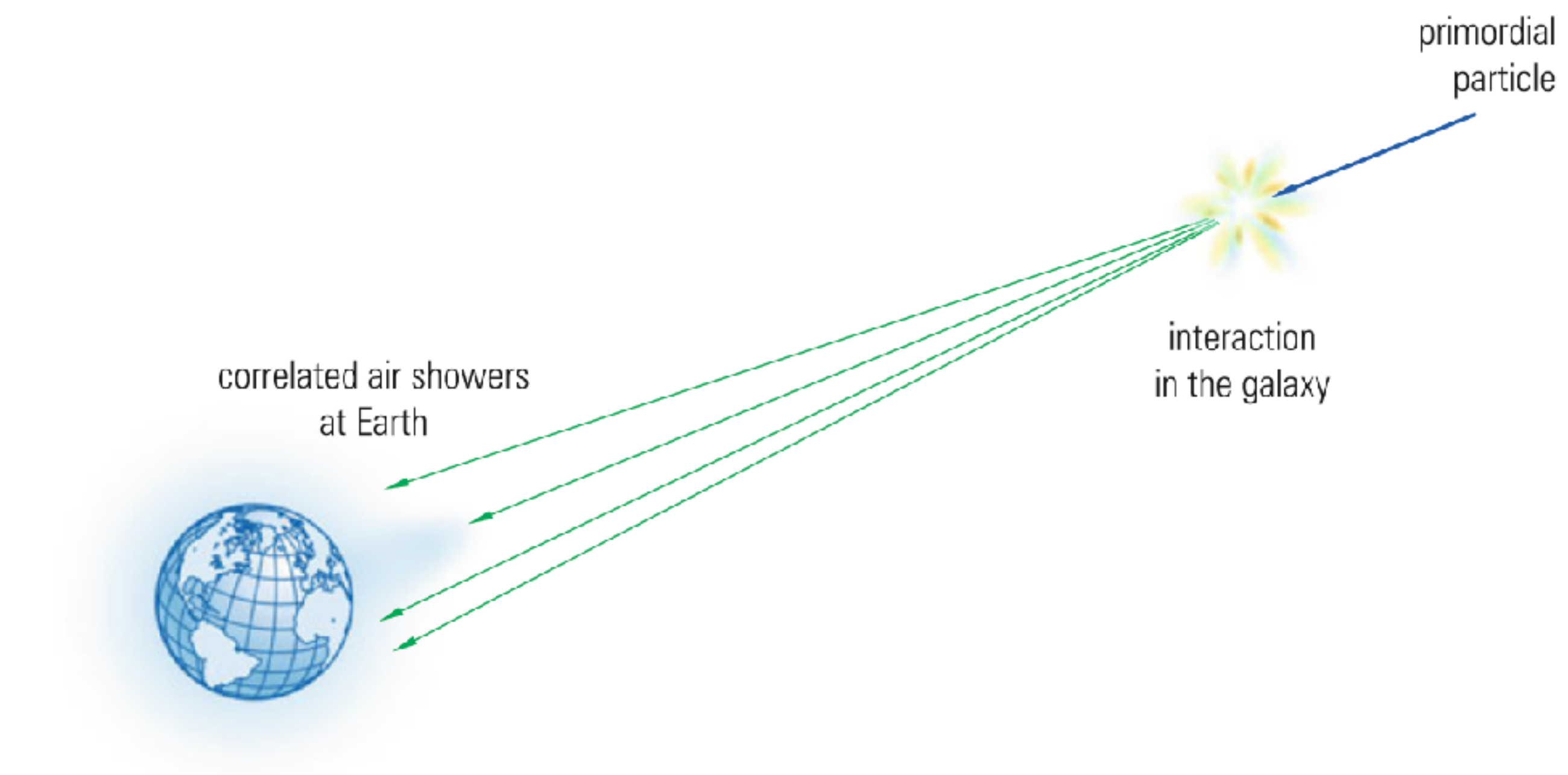


**Fig. 7.38** Possible explanation for the origin of distant correlated air showers

# Extensive air showers

Even moderate **distances of only one parsec ( $3 \times 10^{16}$  m)** are sufficient to produce separations of air showers at Earth on the order of 100 km (primary energy  $10^{20}$  eV, transverse momenta  $\approx 0.3$  GeV/c).

Variations in arrival times of these showers could be explained by unequal energies of the fragments, which could cause different propagation times.

Galactic or extragalactic **magnetic fields** could also affect the trajectories of the fragments in a different way thus also influencing the arrival times.

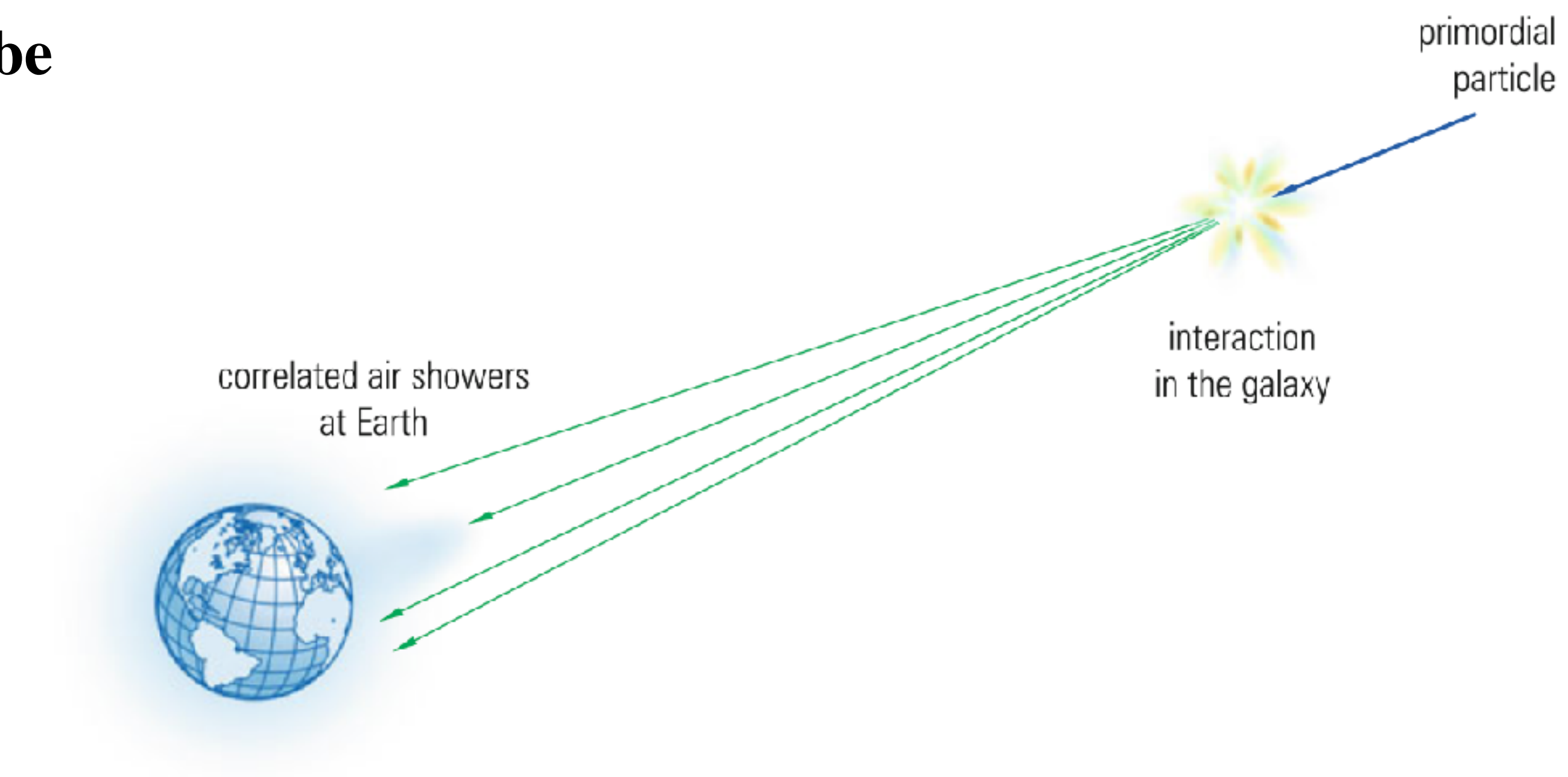


**Fig. 7.38** Possible explanation for the origin of distant correlated air showers

# Radio measurements of air showers

High-energy cosmic rays produce a large number of charged particles when they induce an air shower in the atmosphere. A **primary proton of  $10^{18}$  eV creates about  $10^8$  secondary charged particles at ground level**. At these primary energies **mainly electrons and positrons are produced**, in addition to a much lower number of hadrons and muons. The electrons and positrons of the electromagnetic shower component undergo **various interactions in the atmosphere**. They also **generate synchrotron radiation in the Earth's magnetic field**. Due to their **relatively low energy** this **geosynchrotron emission** is in the radio range. This **radio emission is practically not absorbed in the atmosphere**, and it can be used as a fingerprint of the air shower, which can be **recorded 24h a day**. (Cherenkov radiation and optical fluorescence emission → only during moonless nights)

In addition there are two more mechanisms for the production of radio emission in the atmosphere. As already mentioned the geosynchrotron emission is the dominant mechanism in the weak magnetic field of the Earth. This **geosynchrotron emission is best studied in the frequency range of 40–80 MHz**.

At higher frequencies one would have to live with a considerable background from man-made radio waves. At lower frequencies the radio noise from the Milky Way, generated by synchrotron emission of spiraling electrons in the galactic disk, is a major background. It has also been tried to measure radio emission from air showers in the GHz regime.

# Radio measurements of air showers

Another mechanism, which is important also for dense media, is **the Askaryan effect**. In the course of the shower development **a negative charge excess of 10–20% is generated**. This is a **consequence of the ionization of the air by the air-shower particles**. The ionization electrons essentially follow the cascade, while the much heavier ions stay behind. In the course of shower development this negative charge excess **increases up to the shower maximum and decreases later on**. **This time-dependent negative charge anisotropy creates the emission of radio waves**, like from a time-dependent electric dipole. This radio emission is named after G. Askaryan, who postulated it in 1962.

A third mechanism is **Cherenkov radiation produced by relativistic air-shower electrons and positrons**. Even though the index of refraction of air is very close to unity,  $n = 1.000\ 292$ , still Cherenkov radiation is generated because of the high velocities of the air-shower particles. This **creates Cherenkov radiation in the radio regime and leads to Cherenkov rings with typical radii of about 150 m at ground level for vertical showers**.

Other mechanisms, like bremsstrahlung of electrons and positrons, do not play any role for radio emission.

# Radio measurements of air showers

The Askaryan radiation also known as Askaryan effect is the phenomenon whereby a particle traveling faster than the phase velocity of light in a dense dielectric (such as salt, ice or the lunar regolith) produces a shower of secondary charged particles which contains a charge anisotropy and emits a cone of coherent radiation in the radio or microwave part of the electromagnetic spectrum. The signal is a result of the Cherenkov radiation from individual particles in the shower. Wavelengths greater than the extent of the shower interfere constructively and thus create a radio or microwave signal which is strongest at the Cherenkov angle. The effect is named after Gurgen Askaryan, a Soviet-Armenian physicist who postulated it in 1962.

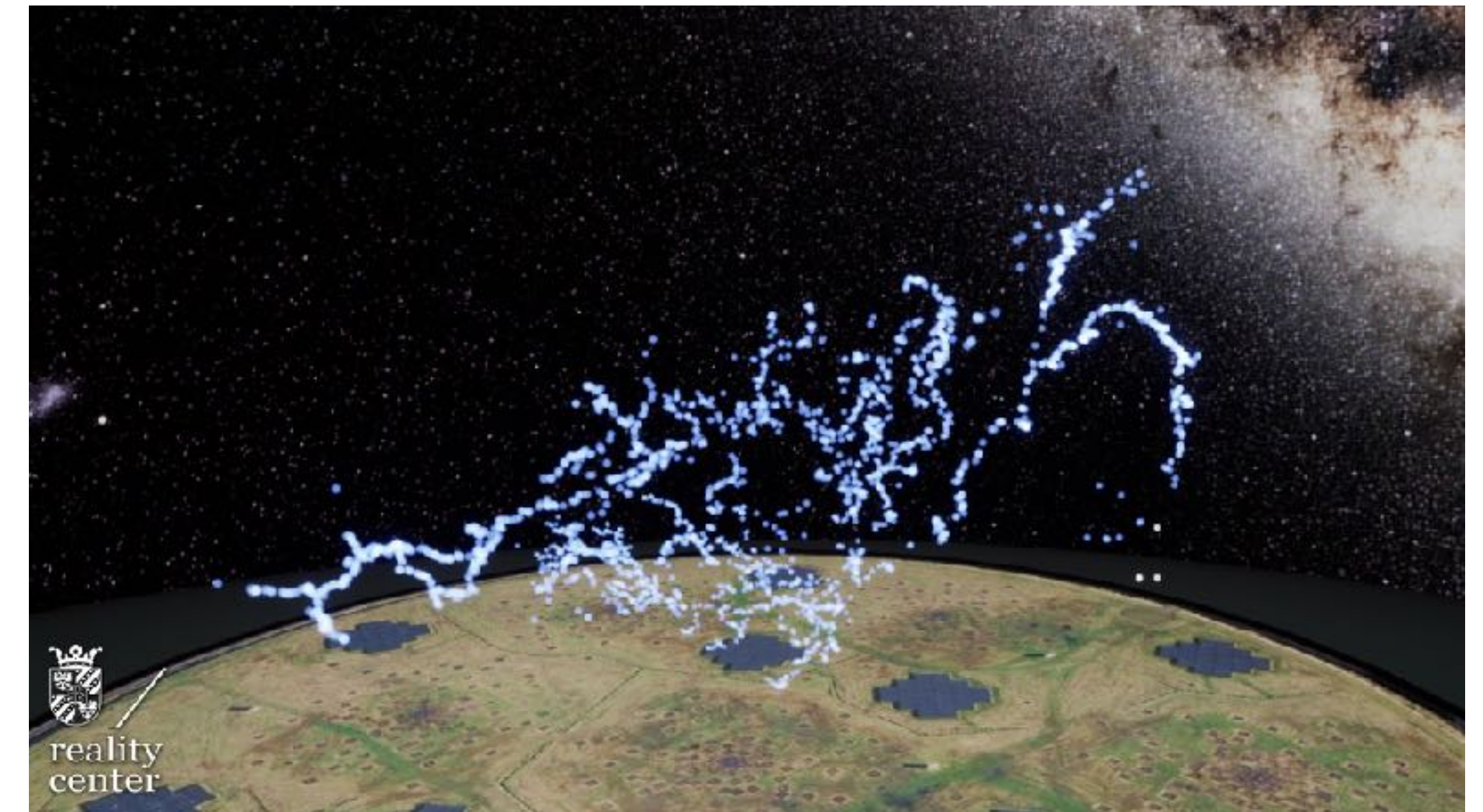
The radiation was first observed experimentally in 2000, 38 years after its theoretical prediction. So far the effect has been observed in silica sand, rock salt, ice, and Earth's atmosphere.

The effect is of primary interest in using bulk matter to detect ultra-high energy neutrinos. The Antarctic Impulse Transient Antenna (ANITA) experiment uses antennas attached to a balloon flying over Antarctica to detect the Askaryan radiation produced as cosmic neutrinos travel through the ice. Several experiments have also used the Moon as a neutrino detector based on detection of the Askaryan radiation.

# Radio measurements of air showers

Radio telescopes can be used to track the development of lightning in the atmosphere. Tracking air showers is very similar to tracking lightning.

**LOFAR (Low Frequency ARray)**

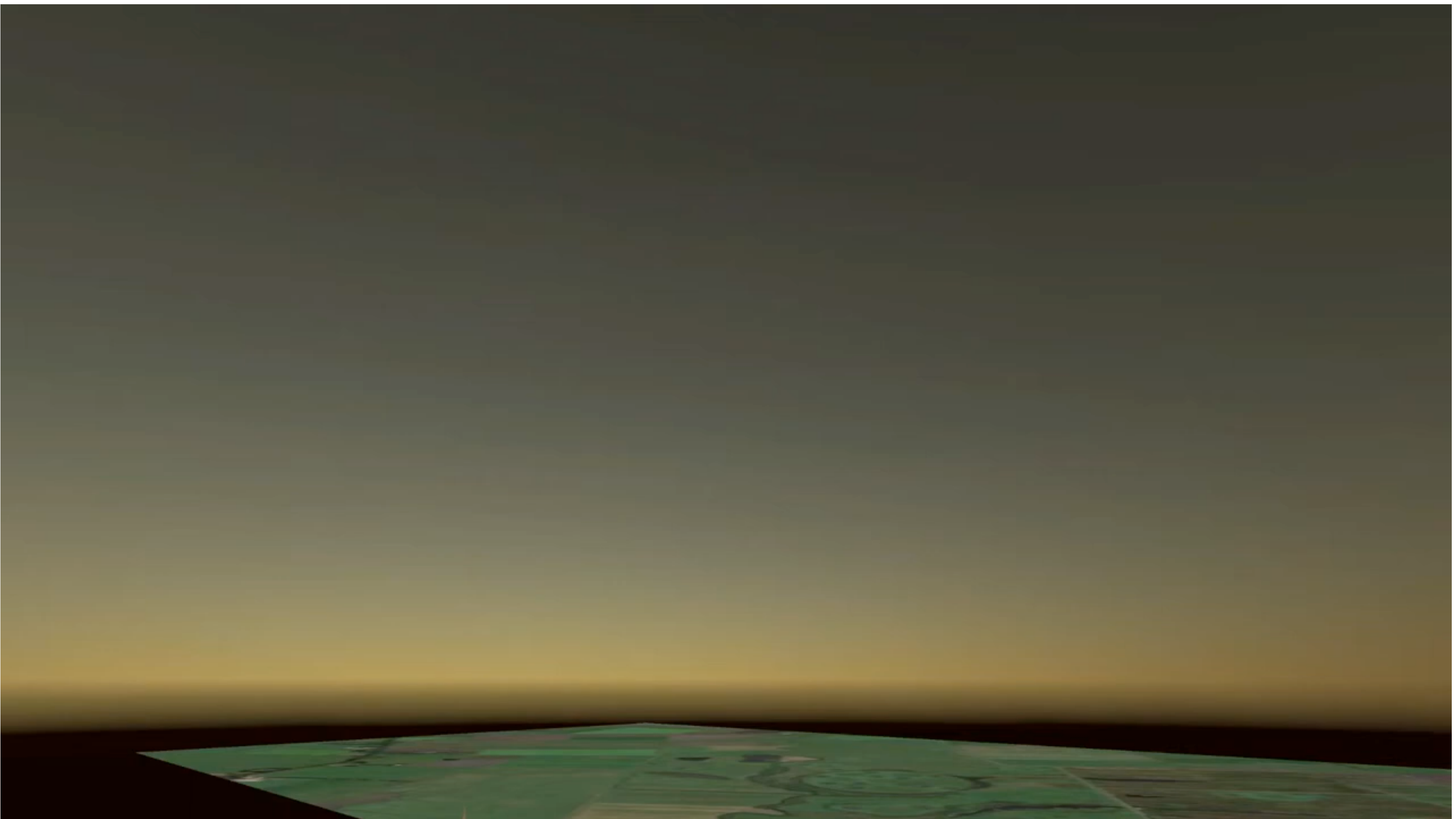


Imaging the path of lightning.

# Radio measurements of air showers

This video is a visualization of a **lightning strike that occurred in 2019**. Each yellow flash indicates the emission of a short radio flash associated to a local flow of charge. The white spheres mark the locations where a flash has occurred and trace out the ionization channels.

Visualization: Stijn Buitink  
Observation & Reconstruction:  
Brian Hare & Olaf Scholten



# Radio measurements of air showers

It has also been tried to measure air showers at frequencies different from the preferred 40-to-80-MHz range. **Measurements in the GHz regime were quite successful**, but did not achieve the quality and significance of the standard techniques in the 40-to-80-MHz range.

The big advantage of radio detection of air showers is that **the radio signal is proportional to the energy of the primary particle**. On top of that **the complete longitudinal development of the cascade in the atmosphere is recorded**. This also supplies the **measurement of the position of the shower maximum**, which is **sensitive to the mass of the primary particle**. A determination of the chemical composition of primary cosmic rays with classical surface detector arrays is particularly difficult.

In the first measurements of radio emission of extensive air showers the radio antennas were rather simple providing only analogue information. The availability of modern fast digital electronics at affordable prices around the year 2000 revived the radio technique for the detection of air showers.



**Fig. 7.39** Inverted dipole of the LOPES experiment in the KASCADE-Grande air-shower detector. In the background several measurement stations are visible, which were used to trigger the readout of the radio signals [137]

# Radio measurements of air showers

A typical detector for radio measurements of extensive air showers consists of **a (large) number of antennas**, which pick up individual radio signals. If possible, the antennas should also **measure all three polarization components** of the radio field. The **lateral width of the radio signal is quite limited** because the radio photons are emitted under relatively small angles with respect to the shower axis. Therefore **separations of the radio antennas of about 100 meter** are favoured. The antennas can be comparatively simple, they must, however, provide a **very accurate timing to enable a good reconstruction of the shower axis** (see Fig. 7.39). The **reconstruction of the shower axis is based on a correlation technique** using the individual signals of all antennas. This beam-forming method also permits to suppress effectively the noise generated by background sources.



**Fig. 7.39** Inverted dipole of the LOPES experiment in the KASCADE-Grande air-shower detector. In the background several measurement stations are visible, which were used to trigger the readout of the radio signals [137]

# Radio measurements of air showers

Usually such radio arrays are **operated jointly with classical air-shower detectors**, which can also provide a trigger for the **readout of the radio antennas**.

A self-triggering radio experiment has to meet the challenge of overcoming the generally high back-ground noise level. In radio-quiet surroundings such a self-triggering mode should be possible.

Figure 7.40 shows the **radio signal of an air shower** as it is obtained from the optimized correlation (beam forming) of 10 antennas of the **LOPES experiment as part of the KASCADE-Grande air-shower array**.



Fig. 7.39 Inverted dipole of the LOPES experiment in the KASCADE-Grande air-shower detector. In the background several measurement stations are visible, which were used to trigger the readout of the radio signals [137]

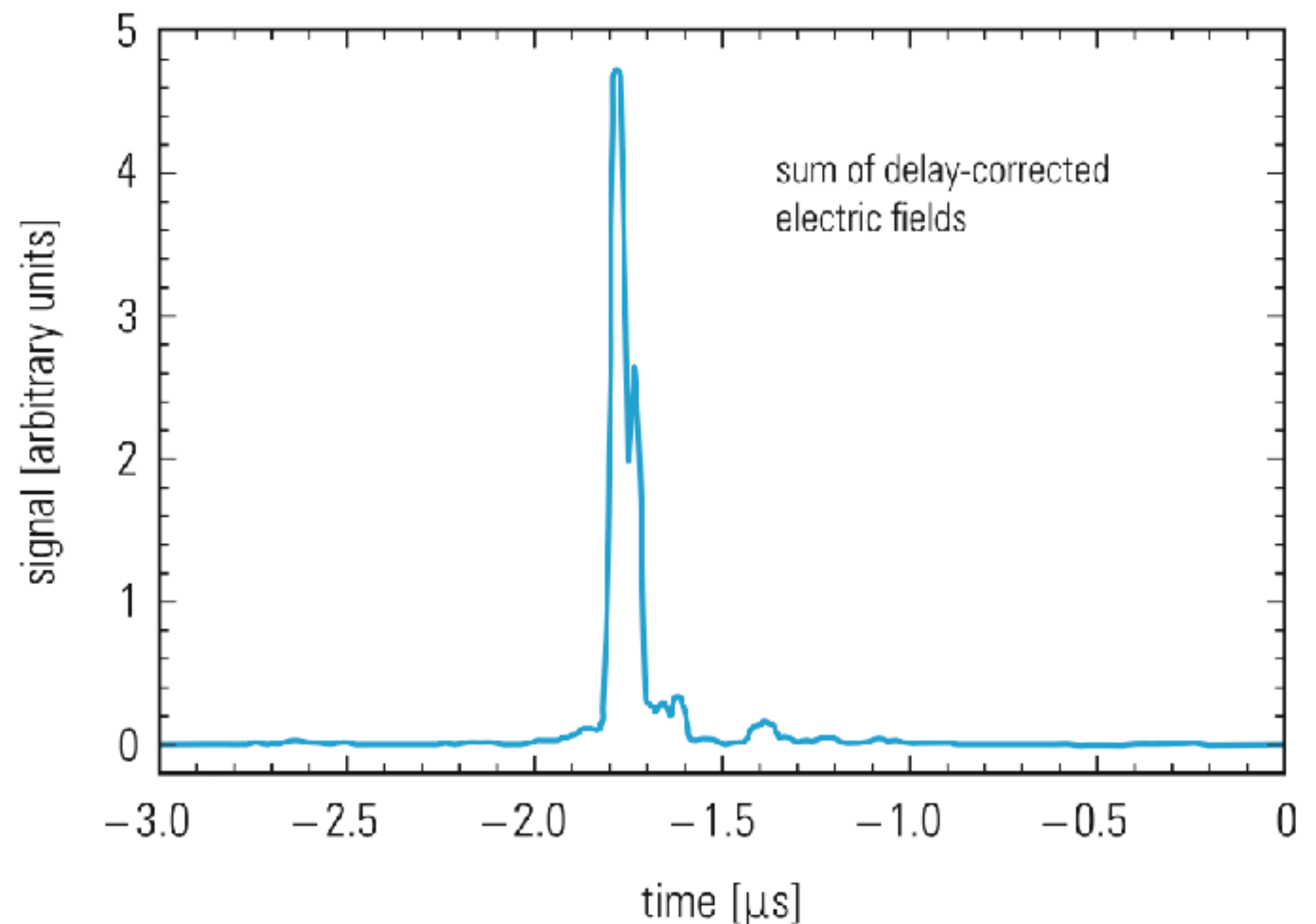


Fig. 7.40 Sum of the ten LOPES antennas by synchronizing and correlating the radio signals in the KASCADE-Grande experiment [137, 138]

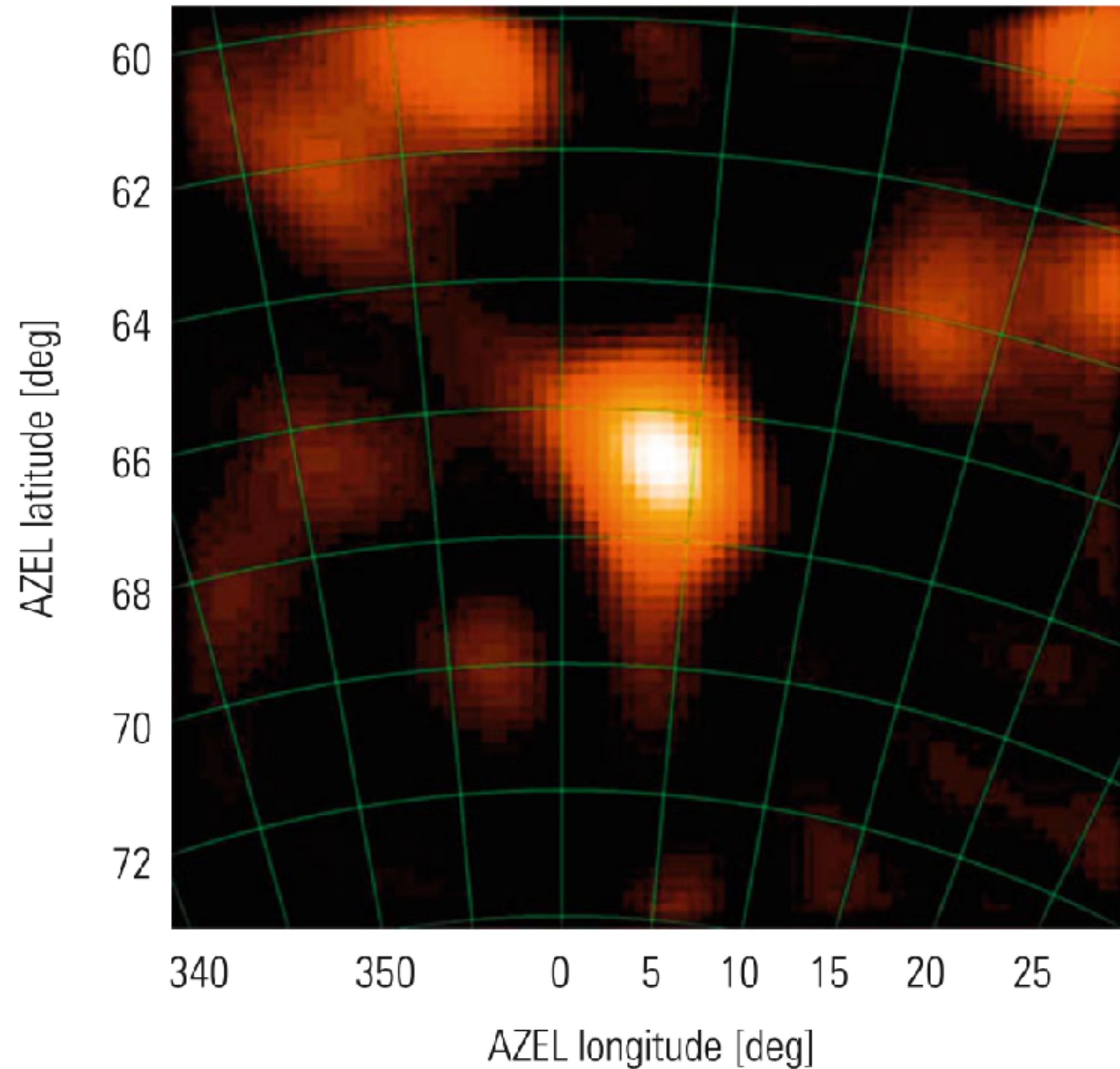
# Radio measurements of air showers

Figure 7.41 shows a **radio map of an air shower event**.

The bright central blob has been reconstructed from the signals of the LOPES experiment operated jointly with KASCADE-Grande. Weak signals in the upper part of the figure are artefacts of the reconstruction procedure.



Fig. 7.39 Inverted dipole of the LOPES experiment in the KASCADE-Grande air-shower detector. In the background several measurement stations are visible, which were used to trigger the readout of the radio signals [137].



**Fig. 7.41** False-colour radio map of an air-shower event. The reconstructed image of the shower is seen as bright blob at the center of the figure. Other weak signals surrounding the central brightness maximum result from interferometer side lobes by the sparse radio array of ten antennas and from background noise in the radio signals. AZEL stands for Azimuth and Elevation [136–138].

# Radio measurements of air showers

Figure 7.42 shows the **variation of the radio signal with the primary energy**. The obtained linear relation allows a **clear determination of the primary energy**, which initiates the radio shower.



Fig. 7.39 Inverted dipole of the LOPES experiment in the KASCADE-Grande air-shower detector. In the background several measurement stations are visible, which were used to trigger the readout of the radio signals [137]

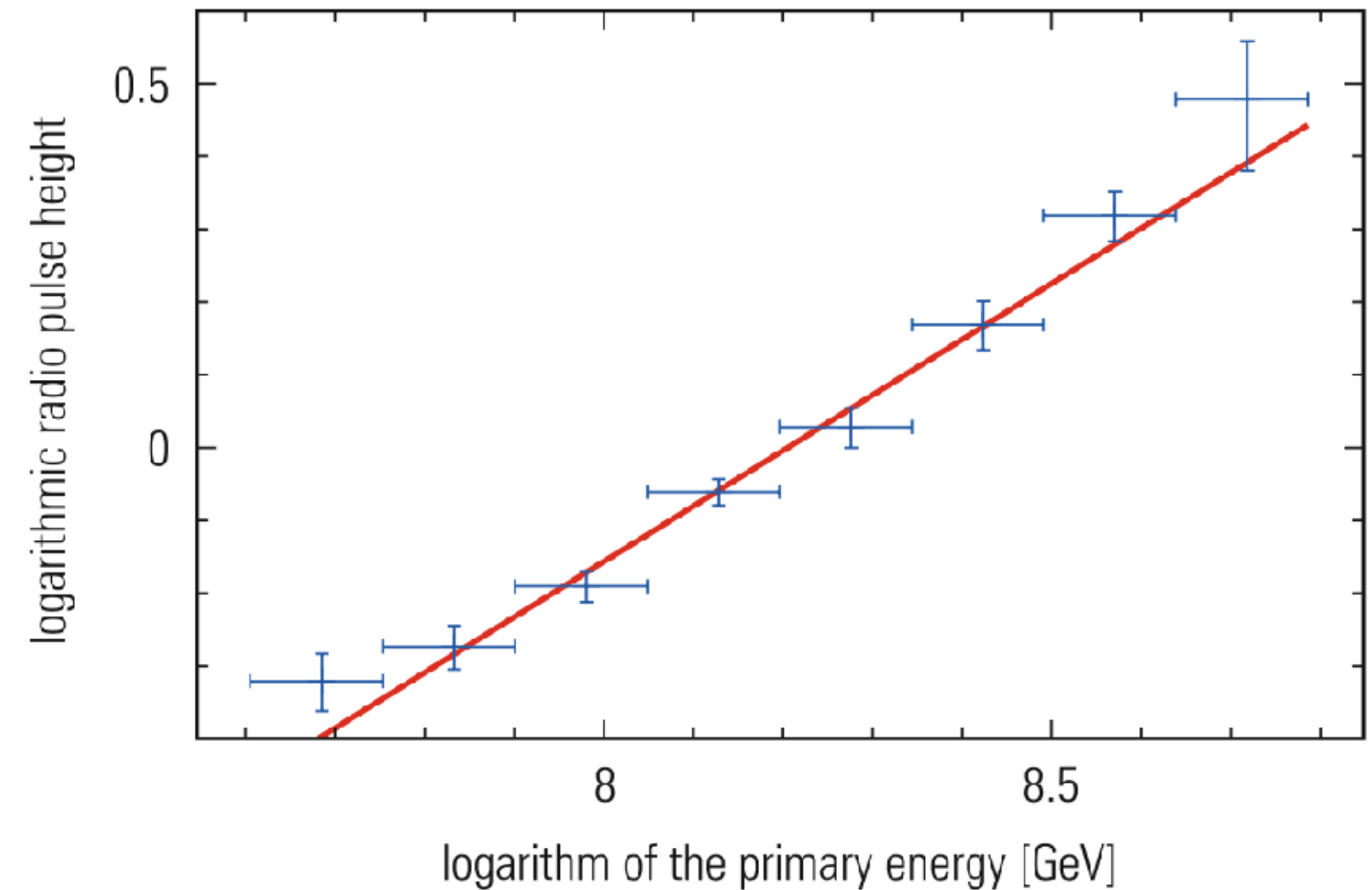


**Fig. 7.42** Variation of the radio signal with the primary energy, as determined by the KASCADE-Grande/LOPES experiments. The shower energy was measured using the classical method with surface scintillation counters. The radio signal from the LOPES experiment was corrected for the angle of the shower axis with respect to the geomagnetic field and to the distance from the shower axis [137, 139]

# Radio measurements of air showers

A very useful advantage of radio measurements of air showers is that they can be **easily modelled**. The different production and propagation processes of radio waves are well understood, and can be reliably described at microscopic level. The possibility of modelling also simplifies the planning and optimization of new radio experiments.

There are **a number of radio arrays taking data, and extensions of existing air-shower experiments** in the planning stage, like Auger in Argentina and at ICECUBE at the South Pole.

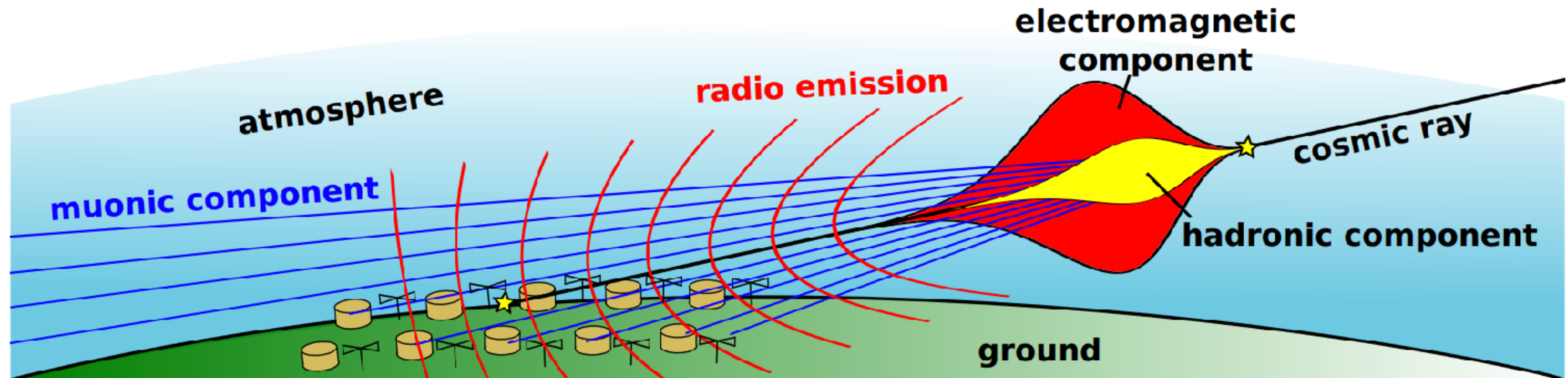


**Figure 4.** Sketch of an inclined air shower. Only muons and the radio emission from the electromagnetic shower component survive until ground. Due to the large size of the radio footprint of inclined showers, the antenna spacing can be of  $o(1 \text{ km})$ , i.e., radio antennas can be placed with the same spacing as particle detectors (from [43])

# Radio measurements of air showers

Radio footprint of an air shower

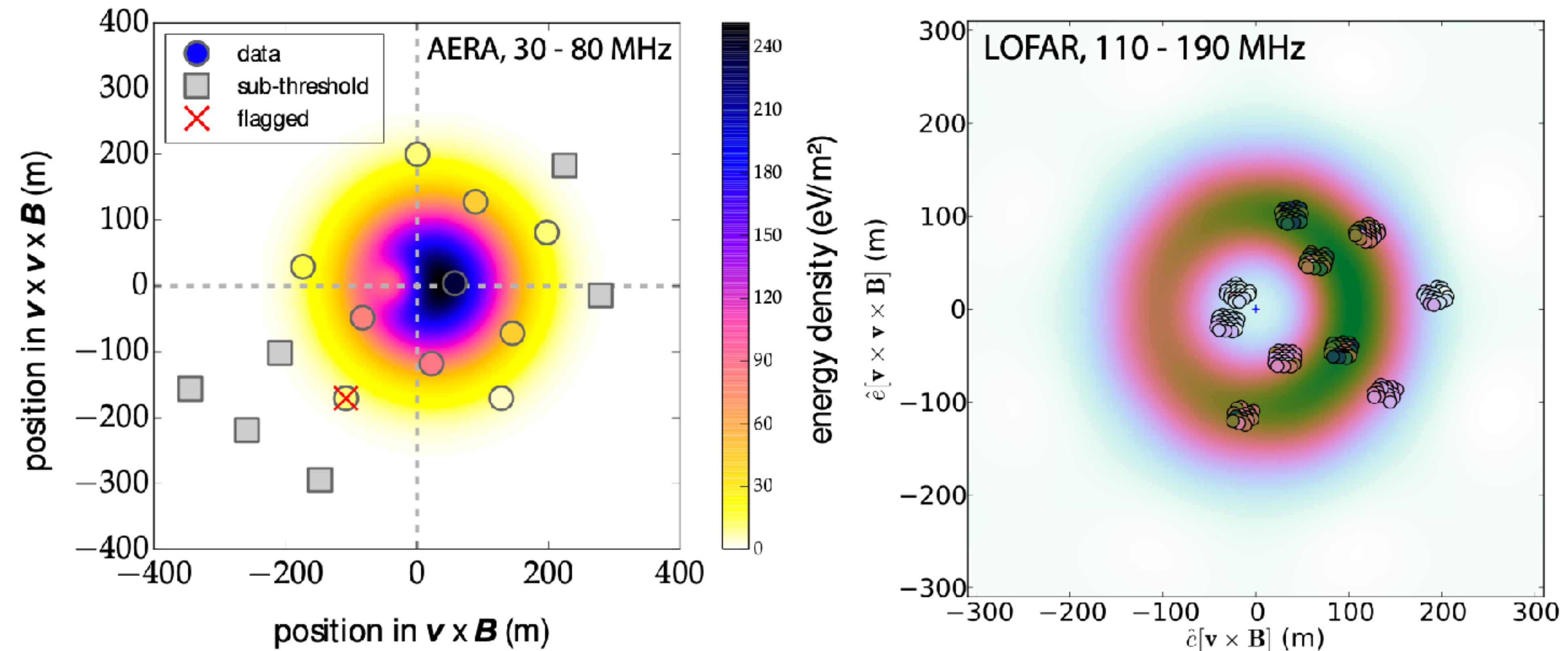


FIG. 2: Footprint of the radio signal in the shower plane in two different frequency bands: left an AERA event measured at 30 – 80 MHz [22], right a LOFAR event measured at 110 – 190 MHz [23]. The color in the circles is the measured signal strength, the surrounding color is a fit of the radio footprint to these measurements. The footprint is slightly asymmetric due to the interference of the geomagnetic and Askaryan effects. The coordinates are along the Lorentz force ( $v \times B$ ) and orthogonal to it ( $v \times v \times B$ ), where  $v$  is the direction of the shower axis and  $B$  the geomagnetic field.

# Radio measurements of air showers

- The **advantage** of radio measurements of air showers is the excellent understanding of simulations, which guarantees reasonable comparability of different experiments. In this way also the uncertainties of antenna calibration can be largely excluded.
- Another big point is the **full-time availability of radio detection of air showers**.
- The good **energy resolution**, and the possibility to identify the nature of the particles initiating the showers via the determination of the position of the shower maximum is also an advantage
- A **disadvantage** is the difficulty to operate self-triggering arrays. This is really a challenge, which might bear fruit in radio-quiet surroundings. In most cases one still needs a trigger from classical air-shower detectors to enable a reliable correlation of background-free low-noise radio signals.

# Acoustic detection of air showers

An **inexpensive alternative** would be the acoustic detection of air showers. **Presently there is a large number of prototype experiments** studying the feasibility of this detection technique for the measurement of high-energy air showers or neutrinos. Acoustic arrays have been installed in IceCube, in the Lake Baikal experiment and in ANTARES and the former NEMO experiment in the Mediterranean Sea. The future KM3NeT neutrino telescope will be equipped with acoustic sensors too.

It has been reported that the US Navy was operating **hydrophones in the ocean** for military purposes, which **have probably detected acoustic signals from air showers**. It is assumed that large showers with energies in excess of,  **$10^{18}$  eV will produce a thermoacoustic shock wave in water or ice** that could be detected by appropriate hydrophones.

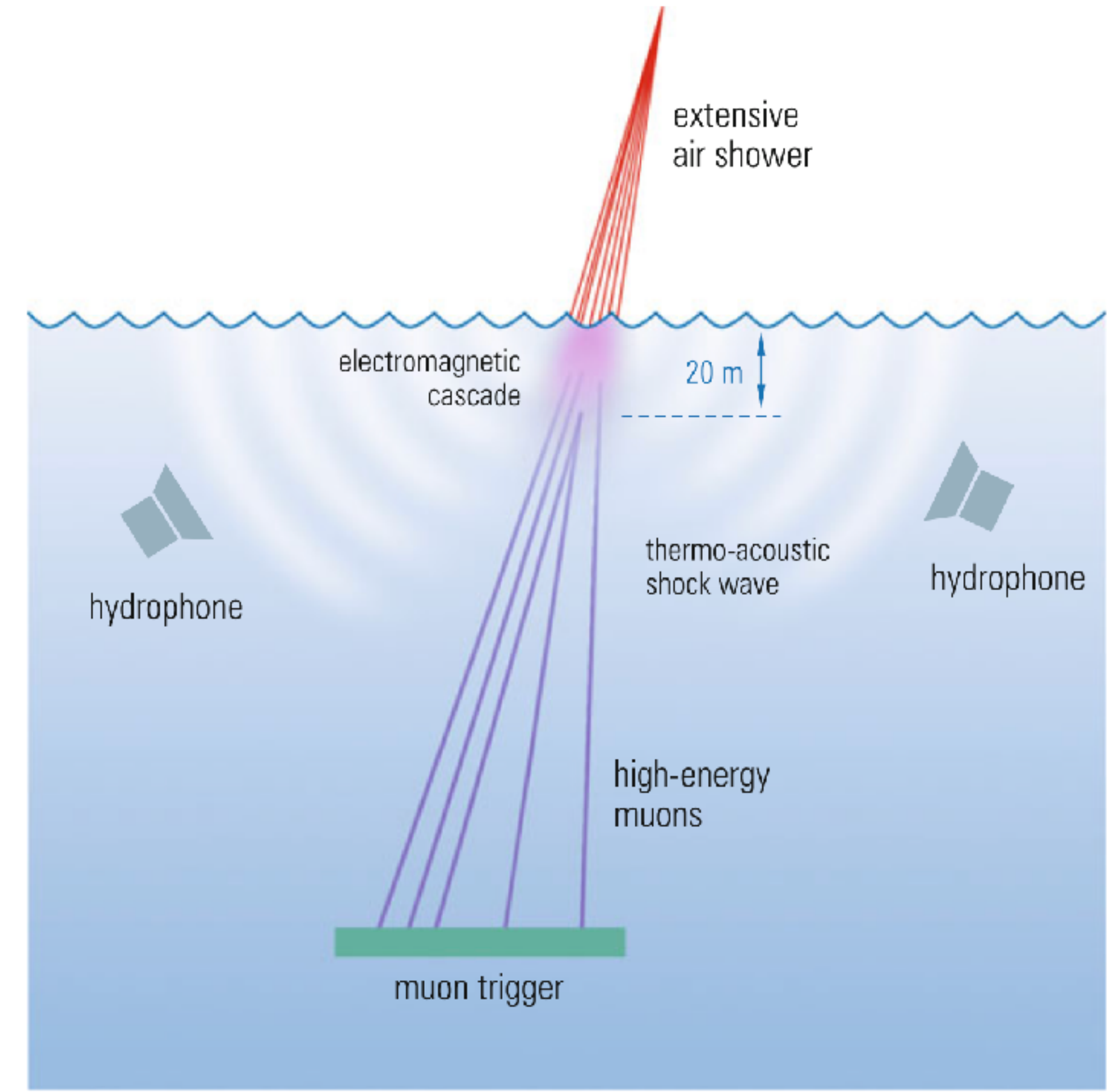


**Fig. 7.43** Sketch demonstrating the principle of high-energy air-shower detection via thermoacoustic shock waves. The electromagnetic component of the shower is absorbed in relatively shallow depths. A possible trigger using energetic muons is indicated [141, 142]

# Acoustic detection of air showers

Accelerator experiments have confirmed the existence of such acoustic shock waves.

The signals are supposed to be **created by the sudden energy deposit of relativistic particles**. In the case of air showers such signals would be **generated by relativistic electrons and positrons, which are absorbed over a relatively short distance in water or ice, which leads to a local heating and a subsequent characteristic pressure pulse that propagates in the surrounding medium**. The acoustic detectors would therefore have to be installed near the surface of such arrays.

Figure 7.43 shows the principle of the acoustic detection method.

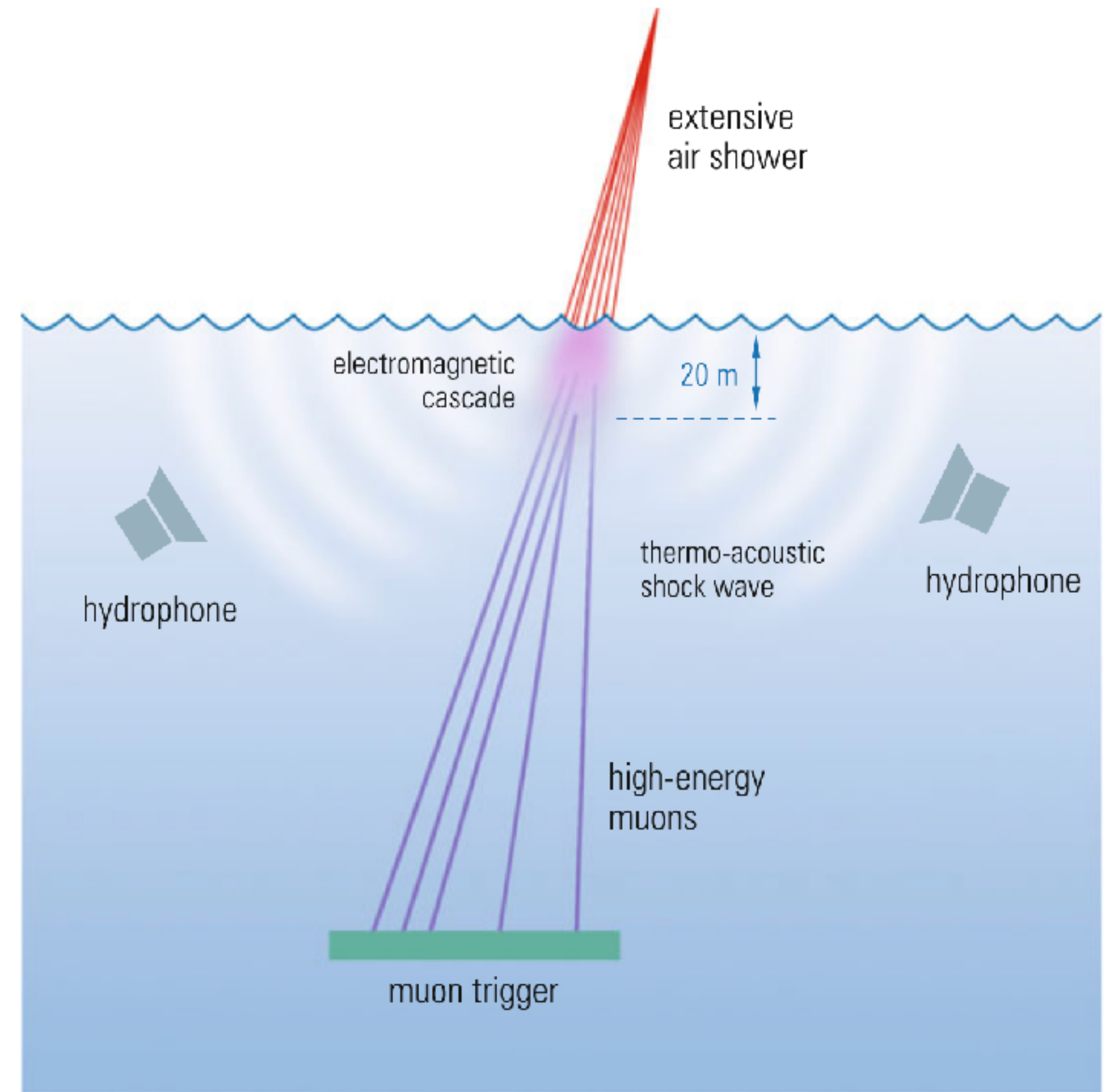


**Fig. 7.43** Sketch demonstrating the principle of high-energy air-shower detection via thermoacoustic shock waves. The electromagnetic component of the shower is absorbed in relatively shallow depths. A possible trigger using energetic muons is indicated [141, 142]

# Acoustic detection of air showers

Fig. 7.44 gives an idea, what an acoustic signal induced by a **high-energy neutrino in water or ice** might look like.

The **advantage** of acoustic detectors is the **very long attenuation length of acoustic signals in water or ice, which would allow large effective volumes to be instrumented**. The **pressure amplitude** of such air showers or neutrino events is expected to be **proportional to the shower energy and inversely proportional to the distance of the hydrophones from the shower core**. The **shower electrons** will deposit their energy over a short distance, which is about **20m in water or ice**.

One of the **problems of acoustic detection is the noise level**. The detection requires high-energy showers beyond  $10^{18}$  eV or even higher. To pick up the acoustic signal in the presence of background a **trigger based of other remnant shower particles would be very helpful** for noise suppression.

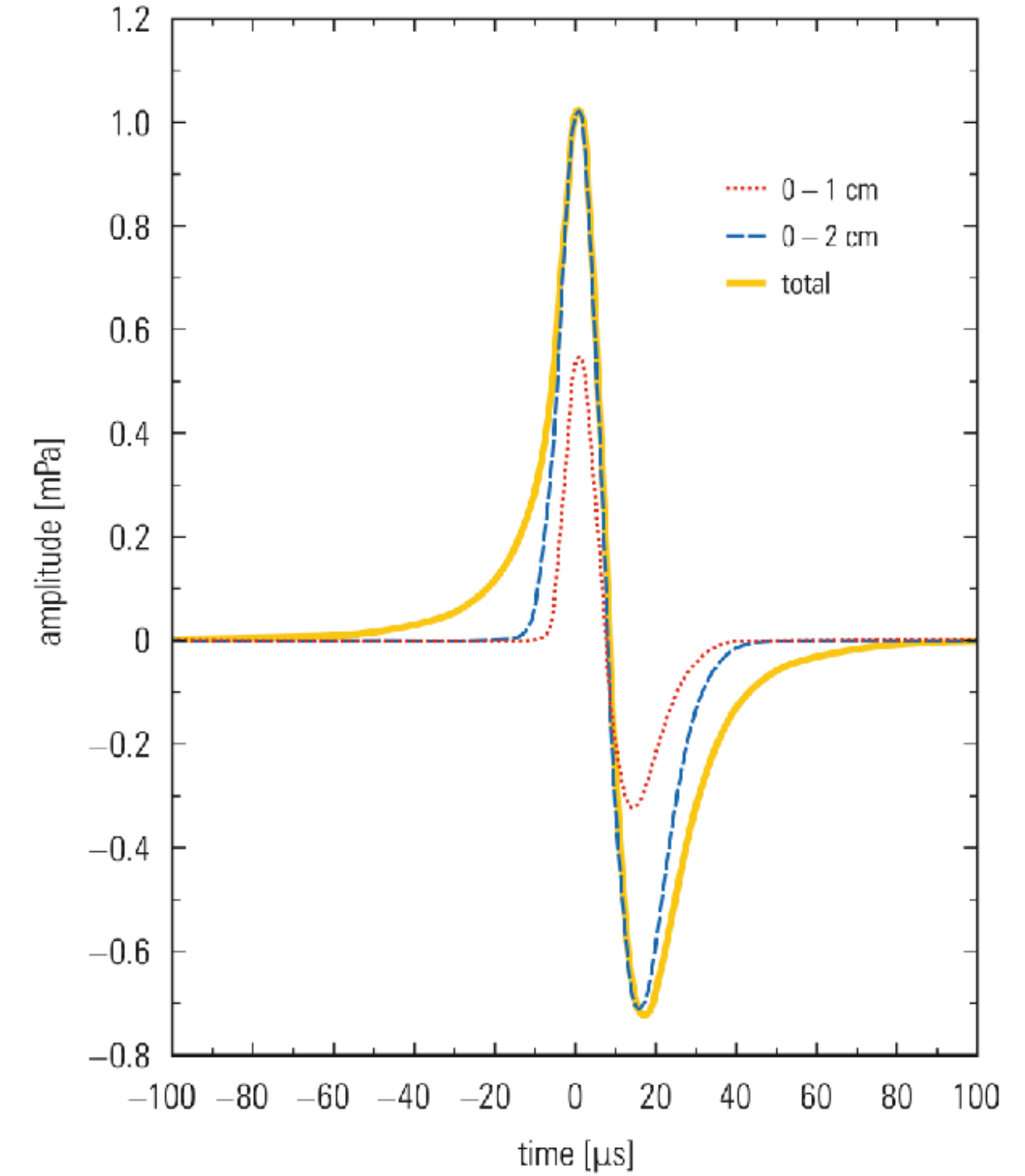


Fig. 7.44 The acoustic signal at a distance of 1 km from the shower axis in the median plane computed from the average of 100 CORSIKA showers each depositing a total energy of  $10^9$  GeV in water. The *dotted*, *dashed*, and *solid* curves show the signals computed from the deposited energies within cores of radius  $1.025$ ,  $2.05$  g/cm $^2$ , and the whole shower (*solid curve*), respectively. It can be seen that most of the amplitude of the signal comes from the energy within a rather small core of radius  $2.05$  g/cm $^2$  [144]

# The most extreme particles

**The most extreme energy cosmic rays - ultra-high-energy cosmic ray (UHECR,  $> 10^{18}$  eV):**

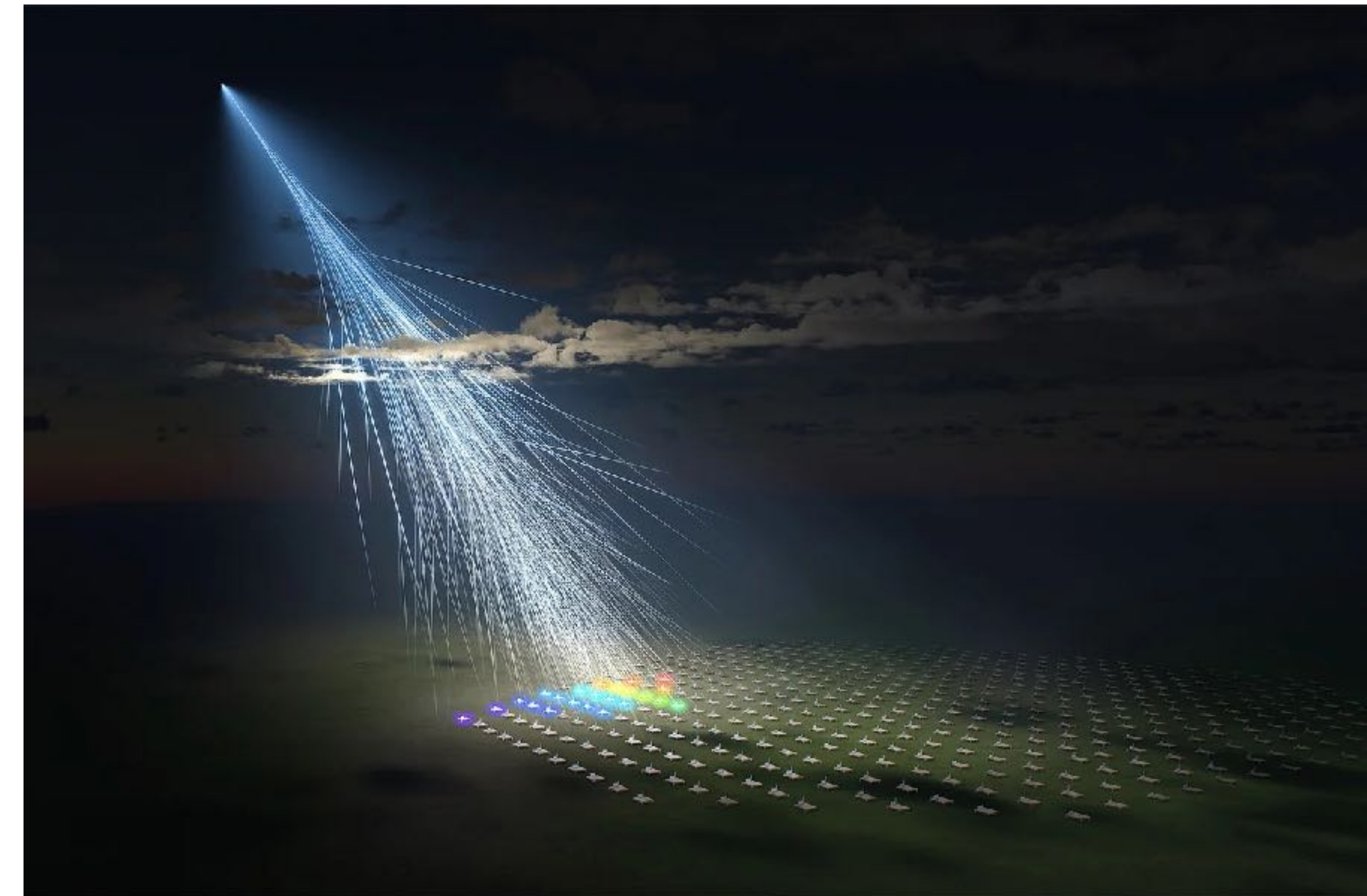
- OMG -  $3.20 \times 10^{20}$  eV
- Amaterashu -  $2.44 \times 10^{20}$  eV

Both were detected in Utah.

Utah's flat terrain and dark skies make it the Northern Hemisphere hub for UHECR detectors. In the Southern Hemisphere the Pierre Auger Observatory complements the observations.

## Questions:

- What type of particle were they? A proton or an iron nucleus?
- Where did they come from? No obvious source, but likely an AGN.



# Problems

8. How many Cherenkov photons in the radio domain (40–80 MHz) are emitted by a relativistic electron in the atmosphere per meter?

# Problems

10. Work out the number of synchrotron photons in the radio range (around 60 MHz), which are produced by a 100-MeV air-shower electron over a distance of 100 m in the Earth's magnetic field. Hint(s): See [151].